

**The Thermal Conductivity
of the High Temperature Superconductor
 $YBa_2Cu_3O_{7-\delta}$**

by

Gold Ziv
Department of Physics, McGill University
Montréal, Québec
Canada

A Thesis submitted to the
Faculty of Graduate Studies and Research
in partial fulfillment of the requirements for the degree of
Master in Science

© Gold Ziv, 1994

Name Gold Riv

Dissertation Abstracts International is arranged by broad, general subject categories. Please select the one subject which most nearly describes the content of your dissertation. Enter the corresponding four-digit code in the spaces provided.

Solid State

0611

U·M·I

SUBJECT TERM

SUBJECT CODE

Subject Categories

THE HUMANITIES AND SOCIAL SCIENCES

COMMUNICATIONS AND THE ARTS

Architecture 0729
 Art History 0377
 Cinema 0900
 Dance 0378
 Fine Arts 0357
 Information Science 0723
 Journalism 0391
 Library Science 0399
 Mass Communications 0708
 Music 0413
 Speech Communication 0459
 Theater 0465

Psychology 0525
 Reading 0535
 Religious Sciences 0714
 Secondary 0533
 Social Sciences 0534
 Sociology of 0340
 Special 0529
 Teacher Training 0530
 Technology 0710
 Tests and Measurements 0288
 Vocational 0747

EDUCATION

General 0515
 Administration 0514
 Adult and Continuing 0516
 Agricultural 0517
 Art 0273
 Bilingual and Multicultural 0282
 Business 0688
 Community College 0275
 Curriculum and Instruction 0727
 Early Childhood 0518
 Elementary 0524
 Finance 0277
 Guidance and Counseling 0519
 Health 0680
 Higher 0745
 History of 0520
 Home Economics 0278
 Industrial 0521
 Language and Literature 0279
 Mathematics 0280
 Music 0522
 Philosophy of 0998
 Physical 0523

LANGUAGE, LITERATURE AND LINGUISTICS

Language
 General 0679
 Ancient 0289
 Linguistics 0290
 Modern 0291
 Literature
 General 0401
 Classical 0294
 Comparative 0295
 Medieval 0297
 Modern 0298
 African 0316
 American 0591
 Asian 0305
 Canadian (English) 0352
 Canadian (French) 0355
 English 0593
 Germanic 0311
 Latin American 0312
 Middle Eastern 0315
 Romance 0313
 Slavic and East European 0314

PHILOSOPHY, RELIGION AND THEOLOGY

Philosophy 0422
 Religion
 General 0318
 Biblical Studies 0321
 Clergy 0319
 History of 0320
 Philosophy of 0322
 Theology 0469

SOCIAL SCIENCES

American Studies 0323
 Anthropology
 Archaeology 0324
 Cultural 0326
 Physical 0327
 Business Administration
 General 0310
 Accounting 0272
 Banking 0770
 Management 0454
 Marketing 0338
 Canadian Studies 0385
 Economics
 General 0501
 Agricultural 0503
 Commerce Business 0505
 Finance 0508
 History 0509
 Labor 0510
 Theory 0511
 Folklore 0358
 Geography 0366
 Gerontology 0351
 History
 General 0578

Ancient 0579
 Medieval 0581
 Modern 0582
 Black 0328
 African 0331
 Asia, Australia and Oceania 0322
 Canadian 0334
 European 0335
 Latin American 0336
 Middle Eastern 0333
 United States 0337
 History of Science 0585
 Law 0398
 Political Science
 General 0615
 International Law and Relations 0616
 Public Administration 0617
 Recreation 0814
 Social Work 0452
 Sociology
 General 0626
 Criminology and Penology 0627
 Demography 0938
 Ethnic and Racial Studies 0631
 Individual and Family Studies 0628
 Industrial and Labor Relations 0629
 Public and Social Welfare 0630
 Social Structure and Development 0700
 Theory and Methods 0344
 Transportation 0709
 Urban and Regional Planning 0999
 Women's Studies 0453

THE SCIENCES AND ENGINEERING

BIOLOGICAL SCIENCES

Agriculture
 General 0473
 Agronomy 0285
 Animal Culture and Nutrition 0475
 Animal Pathology 0476
 Food Science and Technology 0359
 Forestry and Wildlife 0478
 Plant Culture 0479
 Plant Pathology 0480
 Plant Physiology 0817
 Range Management 0777
 Wood Technology 0746
 Biology
 General 0306
 Anatomy 0287
 Biostatistics 0308
 Botany 0309
 Cell 0379
 Ecology 0329
 Entomology 0353
 Genetics 0369
 Limnology 0793
 Microbiology 0410
 Molecular 0307
 Neuroscience 0317
 Oceanography 0416
 Physiology 0433
 Radiation 0821
 Veterinary Science 0778
 Zoology 0472
 Biophysics
 General 0786
 Medical 0760

Geodesy 0370
 Geology 0372
 Geophysics 0373
 Hydrology 0388
 Mineralogy 0411
 Paleobotany 0345
 Paleocology 0426
 Paleontology 0418
 Paleozoology 0985
 Palynology 0427
 Physical Geography 0368
 Physical Oceanography 0415

HEALTH AND ENVIRONMENTAL SCIENCES

Environmental Sciences 0768
 Health Sciences
 General 0566
 Audiology 0300
 Chemotherapy 0992
 Dentistry 0567
 Education 0350
 Hospital Management 0769
 Human Development 0758
 Immunology 0982
 Medicine and Surgery 0564
 Mental Health 0347
 Nursing 0569
 Nutrition 0570
 Obstetrics and Gynecology 0380
 Occupational Health and Therapy 0354
 Ophthalmology 0381
 Pathology 0571
 Pharmacology 0419
 Pharmacy 0572
 Physical Therapy 0382
 Public Health 0573
 Radiology 0574
 Recreation 0575

Speech Pathology 0460
 Toxicology 0383
 Home Economics 0386

PHYSICAL SCIENCES

Pure Sciences
 Chemistry
 General 0485
 Agricultural 0749
 Analytical 0486
 Biochemistry 0487
 Inorganic 0488
 Nuclear 0738
 Organic 0490
 Pharmaceutical 0491
 Physical 0494
 Polymer 0495
 Radiation 0754
 Mathematics 0405
 Physics
 General 0605
 Acoustics 0986
 Astronomy and Astrophysics 0606
 Atmospheric Science 0608
 Atomic 0748
 Electronics and Electricity 0607
 Elementary Particles and High Energy 0798
 Fluid and Plasma 0759
 Molecular 0609
 Nuclear 0610
 Optics 0752
 Radiation 0756
 Solid State 0611
 Statistics 0463

Applied Sciences

Applied Mechanics 0346
 Computer Science 0984

Engineering
 General 0537
 Aerospace 0538
 Agricultural 0539
 Automotive 0540
 Biomedical 0541
 Chemical 0542
 Civil 0543
 Electronics and Electrical 0544
 Heat and Thermodynamics 0348
 Hydraulic 0545
 Industrial 0546
 Marine 0547
 Materials Science 0794
 Mechanical 0548
 Metallurgy 0743
 Mining 0551
 Nuclear 0552
 Packaging 0549
 Petroleum 0765
 Sanitary and Municipal System Science 0790
 Geotechnology 0428
 Operations Research 0796
 Plastics Technology 0795
 Textile Technology 0994

PSYCHOLOGY

General 0621
 Behavioral 0384
 Clinical 0622
 Developmental 0620
 Experimental 0623
 Industrial 0624
 Personality 0625
 Physiological 0989
 Psychobiology 0349
 Psychometrics 0632
 Social 0451

EARTH SCIENCES

Biogeochemistry 0425
 Geochemistry 0996



Abstract

Previous measurements show that the thermal conductivity of $YBa_2Cu_3O_{7-\delta}$ in the basal plane is anisotropic with a large peak in the superconducting state. The magnitude of this anisotropy in the superconducting and normal states, and the dominant mechanism for heat conduction in the superconducting state are currently the subject of debate. We have measured the thermal conductivity of high quality $YBa_2Cu_3O_{7-\delta}$ for deoxygenated, twinned and detwinned samples along the a and b axes to shed light on this issue. We were able to measure the electrical and thermal conductivity using the same contacts and hence determine the Lorenz number $L = \kappa\rho/T$ accurately.

Attributing the normal state anisotropy in the heat transport to electrons in the Cu-O chains, the Lorenz number takes on its full Sommerfeld value i.e. $L = L_0$. Under this assumption, the phonon conduction is about the same in the superconducting and deoxygenated samples.

Our results are discussed in connection with the two possible mechanisms for heat conduction in the superconducting state. We find that although a strong case can be made for the "electronic scenario" whereby the peak is due to rapidly increasing electron mean free path below T_c , it is still not compelling at this stage.

In addition, it is found that the thermal conductivity along the a and b axes is isotropic at low temperatures, with a non zero linear term in κ , indicative of some uncondensed electrons as $T \rightarrow 0$. This low temperature isotropy contradicts previous explanations in terms of non-superconducting chains.

Résumé

Des travaux antérieurs ont montré que la conductivité thermique du $YBa_2Cu_3O_{7-\delta}$ dans le plan de base est anisotrope, avec un important pic dans l'état supraconducteur. L'amplitude de cette anisotropie dans l'état normal et l'état supraconducteur, ainsi que le mécanisme dominant de conduction de chaleur dans l'état supraconducteur, font toujours l'objet de discussions. Nous avons mesuré la conductivité thermique d'échantillons de cristaux désoxygénés, maclés et démaclés le long de l'axe a et b dans le but d'éclaircir le sujet. Il nous a été possible de mesurer la conductivité électrique et thermique en utilisant les mêmes contacts et ainsi correctement déterminer le nombre de Lorenz $L = \kappa\rho/T$.

En attribuant l'anisotropie de l'état normal aux électrons des chaînes de Cu-O, le nombre de Lorenz prend sa valeur maximale (de Sommerfeld), i.e. $L = L_0$. Selon cette hypothèse, la conduction phononique est environ la même dans les cristaux à haute T_c et dans les cristaux désoxygénés.

Nos résultats sont discutés en rapprochement avec deux mécanismes possibles de conduction thermique dans l'état supraconducteur. Nous trouvons que même si le "scénario électronique" peut paraître carrément plus vraisemblable (le pic serait alors dû à l'augmentation rapide du libre parcours moyen des électrons sous T_c), il n'est toute fois pas parfaitement satisfaisant.

De plus, les mesures de conductivité thermique aux basses températures le long des axes a et b, avec un terme linéaire non-nul dans κ , indiquent la présence d'électrons non-condensés lorsque $T \rightarrow 0$. Ce comportement isotrope à basse température contredit des travaux antérieurs dont les explications du terme linéaire sont données en termes de chaînes Cu-O non-supraconductrices.

Acknowledgments

To my wife Amalia, for her love and support despite of the many lonely hours.

To my supervisor Professor Louis Taillefer, which I greatly appreciate for his guidance and support throughout the course of my studies, as well as for his patience and understanding.

To Dr. Brett Ellman for his constant support in this project including the many and unusual hours at the lab. His broad knowledge and experience have had a great impact on my progress.

To Robert Gagnon for the aid in every aspect of this work. Without his invaluable knowledge of crystal growth, this work could not have come to this stage.

To Professor Kamran Behnia of Orsay, France, for his collaboration in this project as well as for the interesting discussions on things other than Physics.

To Eric Dufresne, Geoff Soga and Martin Lacasse, many thanks for their aid with the computer system; To Benoit Lussier, Stephane Legault, Bertrand Billon, Judith Mueller, Karim Aguentaou and Eugenia Corvera for their friendship. Special thanks to Eugenia for the support and encouragement to both my family and I, as well as for the aid with the computer system.

To the technicians of the machine shop, Steve and Michel, for their assistance in building up a system out of nothing.

To Cynthia, Paula and Joanne for helping me cope with bureaucracy.

To the federal immigration of Canada for facing me with the frequent challenge of achieving a student visa. Without them, this work could have been written earlier and my (truly) joyful time at McGill would have been shorter.

Contents

Abstract	ii
Résumé	iii
Acknowledgements	iv
List of Figures	vi
1 Introduction	1
1.0.1 Scattering processes	1
1.0.2 The Drude model	2
1.0.3 The Lorenz number	4
1.1 Thermal conductivity of conventional superconductors	9
1.2 The $YBa_2Cu_3O_{7-\delta}$ compound	11
1.3 Thermal conductivity of $YBa_2Cu_3O_{7-\delta}$: A review of the literature	14
2 The Experiment	22
2.1 Sample Preparation	22
2.1.1 Crystal Growth	22
2.1.2 Characterization	24
2.2 The thermal conductivity	30
2.2.1 Dewar and probe	30
2.2.2 Thermometers and heater	31
2.2.3 Thermal conductivity apparatus	33
2.3 Test of Ag sample	37
2.4 Experimental procedures	39
3 Results and Discussion	46
3.1 Results	46
3.2 Discussion	46
3.3 Conclusions	53
References	57

List of Figures

1.1	The Lorenz number of high purity Au, Ag and Cu	5
1.2	The Lorenz number as a function of temperature and purity	6
1.3	A log-log curve of the thermal conductivity of isotopically pure LiF	8
1.4	The ratio $\frac{\kappa_S}{\kappa_N}$ for the case when impurity scattering is dominant	10
1.5	The ratio $\frac{\kappa_S}{\kappa_N}$ for the case when phonon scattering is dominant	10
1.6	κ of lead as an example for the case in which T_c is higher than the temperature of the thermal conductivity peak	12
1.7	κ of indium as an example for the case in which T_c is lower than the temperature of the thermal conductivity peak	12
1.8	Thermal conductivity of NbC	13
1.9	The $YBa_2Cu_3O_{7-\delta}$ unit cell	14
1.10	The thermal conductivity of $YBa_2Cu_3O_{7-\delta}$ detwinned crystal as was measured by Yu <i>et al.</i>	15
1.11	The thermal conductivity of $YBa_2Cu_3O_{7-\delta}$ detwinned crystal as was measured by Cohn <i>et al.</i>	15
1.12	The quantity $ne^2/m\sigma_n(T)$ as an estimate of the quasiparticle scattering rate in $YBa_2Cu_3O_{7-\delta}$ for temperatures close to T_c	19
1.13	The real part of the electrical conductivity extracted from microwave surface resistance.	20
2.1	Schematic representation of twinned $YBa_2Cu_3O_{7-\delta}$	25
2.2	A picture of a small area of a twinned sample as it is seen in the polarized microscope when the polarizer and analyzer are in 45° to each other.	26
2.3	The same zone (of a twinned sample) as the previous figure with the polarizer and the analyzer parallel to each other.	27
2.4	Susceptibility test	28
2.5	The transition temperature by resistivity and susceptibility test	29
2.6	The dewar and the probe	31
2.7	The quantity $\frac{dlnR}{dlnT}$ for Cu as a function of temperature as was measured by us.	32
2.8	The Cu thermometer	33
2.9	A detailed drawing of the thermal conductivity apparatus, and an electric analog with power as current source and temperature as potential	34

2.10	The electrical circuit of the experiment	35
2.11	The measured electrical resistivity of the Ag sample	38
2.12	The Lorenz number as was measured by us before correcting for radiation, and as was measured by others for samples of higher purity	39
2.13	a) The Cu thermometer vs. probe temperature (obtained from Ge/Pt thermometer) while cooling down (circles) and while heating (squares). b) A magnification of the temperature range with the most significant deviation.	40
2.14	Measured electrical resistance of the samples	41
2.15	Time response of A-B channel at 90K of sample B with applied heater current of 0.866mA (Power=0.66mW).	42
2.16	The Voltage difference between the two thermometers, channel A-B of the LIA, before and after applying heat.	44
3.1	Thermal conductivity of all samples	47
3.2	Measured ρ_a for sample A	48
3.3	The Lorenz number of the a axis, $L_a = \frac{\kappa_a \rho_a}{T}$, using the resistivity curve and the linear fit to the resistivity curve, as in the previous figure	49
3.4	$\kappa_b - \kappa_a$ as a function of temperature.	50
3.5	κ/T as a function of temperature in the a and b axes.	52
3.6	κ/T as a function of T^2 in the a and b axes	52

Chapter 1

Introduction

section Basic conduction properties

1.0.1 Scattering processes

At temperature, $T=0$, one of the results of Bloch's theorem is that *electrons in a perfect periodic potential, in spite of the interaction with the fixed lattice of ions, move forever without any degradation of their mean velocity*[1]. In real crystals, however, this periodicity is broken by impurities, isotopic inhomogeneities, structural defects etc. These imperfections of the lattice act as scattering centers (neglecting for a moment scattering of electrons by itself or by phonons) to degrade the infinite conduction of these electrons. These scattering centers are called *static impurities* which in most cases conserve energy in the collision (not true for magnetic impurities however), and at zero temperature are responsible for the residual electrical resistivity.

Heat in insulators, carried by phonons, could also be infinitely well conducted were it not for static imperfections and sample boundaries. However even without these imperfections, one should remember the anharmonic terms in the Hamiltonian will, eventually, degrade the perfect conductivity of the phonons.

At finite T , inelastic collisions become important, and in general, electrons and phonons scatter each other.

On average, every particle, say an electron, travels a mean distance between col-

lisions, called the *mean free path*, and the time between these collisions is called the *relaxation time*, τ . In the general case, when there are more than one scattering mechanism but one does not alter the other, the total scattering rate, $1/\tau$, is the sum of the several scattering rates from different mechanisms, i.e.

$$\tau_{\text{electrons}}^{-1} = \tau_{\text{electrons-imperfections}}^{-1} + \tau_{\text{electrons-phonons}}^{-1} + \tau_{\text{electrons-electrons}}^{-1}$$

Similarly for $1/\tau_{\text{phonons}} = \tau_{\text{ph-imp}}^{-1} + \tau_{\text{ph-el}}^{-1} + \tau_{\text{ph-ph}}^{-1}$. This is called *Mattiasen's Rule*. The validity of this rule relies on a relaxation time, τ , which is independent of the momentum \vec{k} . In formal theories this is not correct but within the relaxation time approximation, this is a valuable tool.

1.0.2 The Drude model

Drude assumed the electrons in a metal are free from interactions except for point collisions with other electrons or with the ions. The electrical current density, hence, is given by the number of carriers times their charge times their mean velocity between collisions. In the presence of an electric field, \vec{E} , each electron has a mean velocity in the direction anti parallel to \vec{E} . Classically the equation of motion between collisions is $\vec{v}_t = \vec{v}_0 - e\vec{E}t/m$. Since in absence of a field the average current is zero, the velocity gained between collisions due to the field is $-e\vec{E}t/m$. Taking t to be short and, on average $t = \tau$, the current density can be written as

$$\vec{j} = \frac{ne^2\tau}{m}\vec{E} \equiv \sigma\vec{E} \quad (1.1)$$

To obtain the electronic thermal conductivity, Drude considered a model in which the electrons move along the x-axis so at a point x half the electrons come from the high temperature side and half from the low temperature side. If $\epsilon(T)$ is the equilibrium thermal energy of the electron, then on average each electron carries the thermal energy of the point where it had its last collision. At point x the electrons that came from the high temperature side had their last collision at $x - v\tau$. Their contribution to the thermal current density is $\frac{n}{2}v\epsilon(T[x - v\tau])$. The electrons coming

from the other side have the same form of current density but with negative velocity. Adding the two terms and expanding around x gives the heat current density

$$j_x^q = \frac{1}{2} n v_x \{ \varepsilon(T[x - v_x \tau]) - \varepsilon(T[x + v_x \tau]) \} = n v_x^2 \tau \frac{d\varepsilon}{dT} \left(-\frac{dT}{dx} \right)$$

On average $\langle v_x^2 \rangle = \frac{1}{3} v^2$ so

$$\vec{j}^q = \frac{1}{3} v^2 \tau c_V (-\nabla T) \equiv \kappa_e (-\nabla T) \quad (1.2)$$

Drude was wrong in taking the classical velocity and specific heat of the electrons. Using the Sommerfeld theory of conduction, $v^2 = v_F^2 = 2\varepsilon_F/m$ and $c_V = \frac{\pi^2}{2} \left(\frac{k_B T}{\varepsilon_F} \right) n k_B$, one concludes

$$\kappa_e = \frac{\pi^2 n k_B^2 \tau}{3 m} T \quad (1.3)$$

Heat can also propagate through the lattice of ions, i.e. by phonons. The thermal conductivity of the phonons can be found by the same formalism as for the electrons, replacing the velocity of the electrons by the sound velocity, c , assuming the Debye approximation for phonon dispersion relation, $\omega = ck$. Hence

$$\kappa_{ph} = \frac{1}{3} c_V c^2 \tau \quad (1.4)$$

The Drude model, although over simplified, gives the right conduction equations to within some corrections. However one cannot proceed much further with this model. A better picture on conduction is given by the relaxation time approximation, for example, in which the relaxation time is taken to be energy dependent and employing the Fermi-Dirac distribution to recover the Drude model to an accuracy of $\left(\frac{k_B T}{\varepsilon_F} \right)^2$ ($\sim 10^{-4}$ at 300K for most metals). One should note that in this model the electron mass comes from the mass tensor $M_{\mu\nu}^{-1}$ so in order to recover the Drude formulas it is necessary to deal with samples of cubic symmetry.

1.0.3 The Lorenz number

The hardest variable in the conduction equations to determine theoretically is the scattering rate τ^{-1} . Dividing the thermal by the electrical conductivity of the electrons, the relaxation time cancels out and one obtains

$$\frac{\kappa_e}{\sigma T} = \frac{\pi^2}{3} \left(\frac{k_B}{e} \right)^2 \equiv L_0 = 2.44 \times 10^{-8} \text{ watt - ohm/K}^2 \quad (1.5)$$

This formula is called the *Wiedemann-Franz law* and the value of L_0 is the *Sommerfeld value* and the ratio $\frac{\kappa_e}{\sigma T}$ is the *Lorenz number*. The Wiedemann-Franz law assumes electrons scatter elastically so the relaxation time, τ , is the same for the electrical and thermal conductivity. However there are scattering processes that can degrade thermal conduction without degrading electrical conduction. Qualitatively, this can be explained by the fact that electrons maintain their charge in a collision so the only way to degrade electrical current is by changing the electron velocity. However the "charge" in the thermal current is replaced by $(\epsilon - \mu)/T$.¹ Therefore if energy is conserved in each collision, the electrical and thermal current will degrade the same. On the other hand, inelastic scattering will cause the Lorenz number to be smaller than L_0 since energy is also used in this case. The Wiedemann-Franz law will hold to a good approximation in two cases: 1) at low temperatures, where inelastic scattering becomes small and the main source of scattering comes from impurities and defects in the lattice, which are elastic scatterers, or 2) at high temperatures where scattering involves large momentum transfer, q , across the Fermi surface (forward scattering) which degrades electrical and thermal conductivity by the same amount [2].

¹This can be seen as follow: under temperature gradient, assume T is constant for a short interval of length, yield the thermodynamic identity $dQ = TdS - \mu dN$. In term of current densities, that is $j^q = j^e - \mu j^n$ where j^e , j^n and j^e (the electrical current density) take the form

$$\begin{pmatrix} j^e \\ j^n \\ j^e \end{pmatrix} = \int \frac{d\vec{k}}{4\pi^3} \begin{pmatrix} \epsilon_{\vec{k}} \\ 1 \\ -e \end{pmatrix} \vec{v}_{\vec{k}} f_{\vec{k}}$$

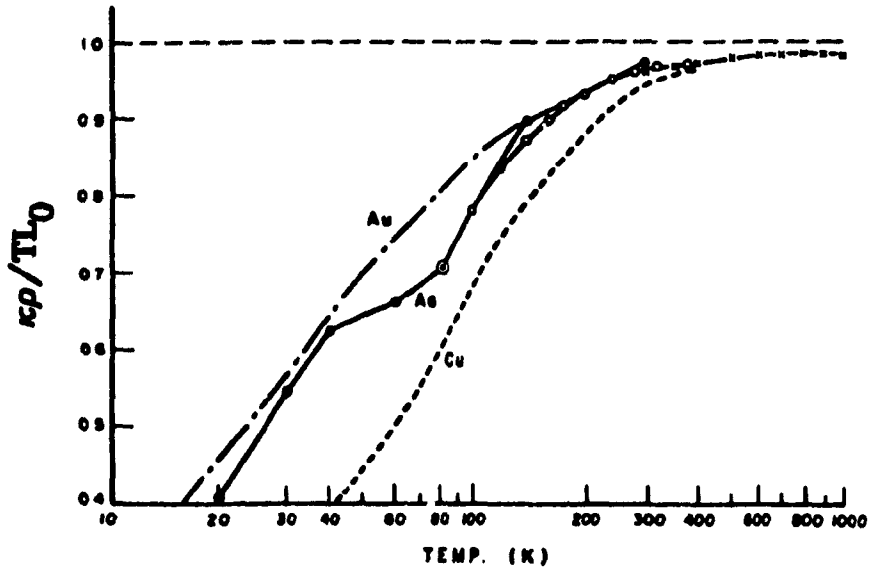


Figure 1.1: The Lorenz number of high purity Au, Ag and Cu (after T. Matsumura *et al.*[3]).

In pure metals, the lattice thermal conductivity is negligibly small compared with the electronic thermal conductivity, so that one can measure directly κ_e , and hence the Lorenz number. Figure 1.1 shows the Lorenz number of Au, Ag and Cu. The strong deviation of the Lorenz number from its calculated L_0 at intermediate temperatures (below about 200K) reveals the importance of the inelastic processes, electron-phonon scattering in this case. It is observed that at high and low temperatures, $L \simeq L_0$. We will use this property later in this work to test the thermal conductivity obtained in our measurements. One should note the variation of the Lorenz number as a function of purity illustrated in figure 1.2: the temperature at which the mean free path, l , becomes comparable to the mean distance between adjacent impurities increases as this mean distance decreases, i.e. as the density of impurities increases.

While the electrical conductivity in the Wiedemann-Franz law is measured directly, the measured thermal conductivity is the sum $\kappa_e + \kappa_{ph}$. Some authors make use of this fact to estimate the significance of the phonons in the thermal conductivity of a material by taking the electronic Lorenz value not to exceed L_0 , and attributing the rest to phonons.

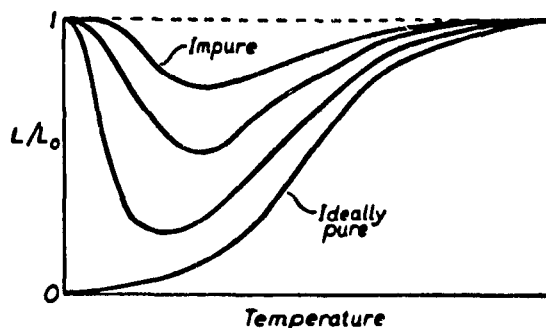


Figure 1.2: The Lorenz number as function of temperature and purity (after H.M. Resenberg, p. 120 [4]).

Let us now discuss the temperature dependence of the thermal conductivity. First, the phonons. For $T \ll \Theta_D$ the heat capacity $c_V \propto T^3$ (in the Debye model) and for temperatures well above Θ_D it is constant (the law of Dulong-Petit). The temperature behavior of the relaxation time is more complicated. At high temperatures ($T \gg \Theta_D$) the dominant phonon process is the phonon-phonon scattering and for a given phonon the scattering rate is linearly proportional to the number of phonons. The number of phonons is given by $n(\mathbf{k}) = \frac{1}{e^{\hbar\omega(\mathbf{k})/k_B T} - 1} \approx \frac{k_B T}{\hbar\omega(\mathbf{k})}$ so $\tau_{ph-ph}^{-1} \sim T$, and

$$\kappa \sim \frac{1}{T^2} \quad (1.6)$$

where α is close to unity (perhaps higher due to anharmonic terms).

As the temperature decreases, the number of phonons decreases however some phonons may still have energy of the order of $\hbar\omega_D$ hence the occupation number of phonons $n(\mathbf{k}) = \frac{1}{e^{\hbar\omega(\mathbf{k})/k_B T} - 1} \approx e^{-\Theta_D/T}$ so that

$$\tau \sim e^{T_0/T} \quad (1.7)$$

As the temperature drops the mean free path increases dramatically until it becomes comparable with the mean free path due to phonon-boundary scattering. Below that temperature the mean free path remains constant but then the cubic term in the heat capacity decreases the thermal conductivity, and $\kappa \sim T^3$. In summary, one should observe an enhancement in the thermal conductivity of insulators as the temperature

decreases from, say Θ_D , with a peak which is related to the impurity concentration (or to sample dimensions in case of very pure samples). Then the thermal conductivity drops to zero as T^3 . This general behavior of the thermal conductivity is illustrated in figure 1.3, for isotopically pure LiF[5].

In a non-insulating crystal, phonons can be scattered by electrons. Since only electrons within $k_B T$ of the Fermi energy, ϵ_F , can participate in the process, the number of these electrons is $\frac{k_B T}{\epsilon_F}$, and hence $\tau_{ph-el}^{-1} \sim T$. In the temperature range where $c_V \sim T^3$, $\kappa_{ph-el} \sim T^2$. According to Mattiessen's rule and the fact that $\tau_{ph-boundaries}$ is constant at these low temperatures, the phonon thermal conductivity is

$$\kappa_{ph} \sim c_V \tau = \left(\alpha/T^2 + \beta/T^3 \right)^{-1} \quad (1.8)$$

The temperature behavior of the thermal conductivity of the electrons can also be derived. In the temperature range where the heat capacity of the phonons, $c_V = \frac{dE}{dT} \sim T^3$, the total crystal energy, $E \sim T^4$. Since the average energy of the phonon is of the order of $k_B T$, the number of phonons is proportional to T^3 and so is τ_{el-ph}^{-1} . From Mattiessen's rule and equation 1.3, assuming $\tau_{el-impurity}$ to be constant,

$$\kappa_e = \left(\frac{A}{T} + BT^2 \right)^{-1} \quad (1.9)$$

For our discussion it is important to note that equation 1.9 can be written as $\frac{\kappa_e}{T} = (A + BT^3)^{-1}$ so when $T \rightarrow 0$, $\frac{\kappa_e}{T}$ intercepts to a non-zero value.

This section describes the expected behavior of the conduction of heat either by electrons or phonons. In many cases neither one of them is negligible. Since the measured thermal conductivity of the crystal is the sum of two contributions, $\kappa = \kappa_{el} + \kappa_{ph}$, it is hard to separate between the two. One way to do so is to fit the measured thermal conductivity, $\kappa_{measured}(T)$ to equations 1.8 and 1.9.

We shall make use of the Wiedemann-Franz law to estimate an upper limit of the electronic contribution. We shall find that in good crystals of $YBa_2Cu_3O_{7-\delta}$ (with $\delta \approx 0$) this upper limit is about 30% - 45% of the total thermal conductivity, hence

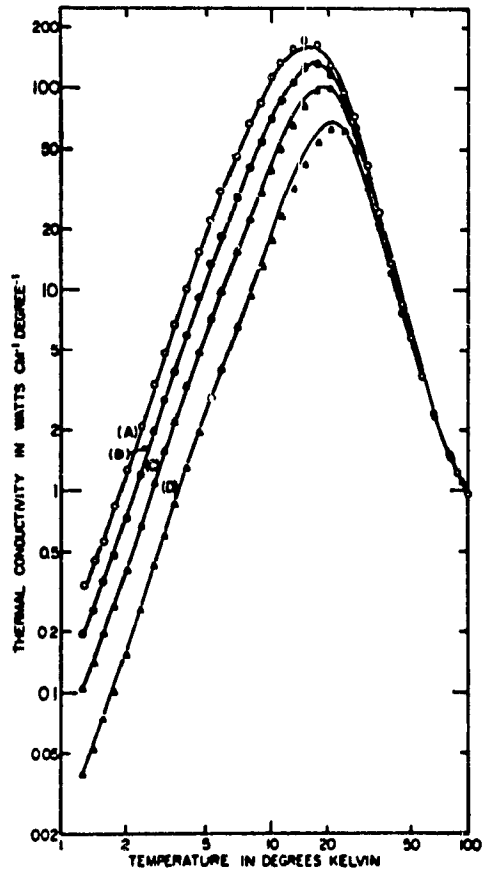


Figure 1.3: A log-log curve of the thermal conductivity of isotopically pure LiF [5]. Below $\sim 10\text{K}$ the thermal conductivity is limited by surface scattering (the difference between the sizes of the samples is reflected in the different values at low temperatures) and the temperature dependence comes from the T^3 behavior of the specific heat. The thermal conductivity reaches a maximum when the mean free path due to phonon-phonon scattering is comparable to that due to scattering by the surface. At higher temperatures $\tau_{p\lambda}^{-1}$ rapidly increases with temperature while the specific heat starts to level off.

one cannot neglect it.

1.1 Thermal conductivity of conventional superconductors

Early experiments by Onnes and Holst[6] showed that at the superconducting transition point T_c , when the electrical resistance suddenly goes to zero, no discontinuous change in the thermal conductivity occurs. Later it was shown by De Haas and Br emmer[7] and Mendelssohn and Pontius[8] that the thermal conductivity of a superconductor has a lower value than when a magnetic field is applied (to drive it into "normal" state).

A simple model to explain it is the *two fluid model* which assumes that below the transition point, T_c , a certain fraction of the electrons, $1 - x$, remains normal. x was found experimentally[9] to be

$$x = 1 - \left(\frac{T}{T_c}\right)^4 \quad (1.10)$$

The electrical resistivity, is always short-circuited by the superconducting electrons.

Experiments by Daunt and Mendelssohn[16] led to the conclusion that the specific heat of the superconducting electrons is zero hence they can't transport heat and the thermal conductance arises from the normal electrons. As the temperature drops, their number decreases and the thermal conductance decreases faster than in the normal state.

The B.C.S. theory makes use of a formal transport theory and the *Boltzmann equation*² to create an integro-differential equation. The equation for thermal conductivity of electrons limited by electron-impurity scattering is found, by means of variational principle, to be the same as for metals except that the lowest excited state

²The total rate of change $\dot{f}_k = \dot{f}_k|_{diff} + \dot{f}_k|_{field} + \dot{f}_k|_{coll}$ must vanish in the steady state. f is the Fermi-Dirac distribution, $\dot{f}_k|_{diff} = -\left(\frac{\partial f_k}{\partial r}\right)\left(\frac{\partial r}{\partial t}\right) = -\vec{v}_k \frac{\partial f_k}{\partial r}$ and $\dot{f}_k|_{field} = \left(\frac{\partial f_k}{\partial k}\right)\left(\frac{\partial k}{\partial t}\right)$.

The current density is $\Sigma_k \epsilon_k v_k f_k$ as in the previous footnote.

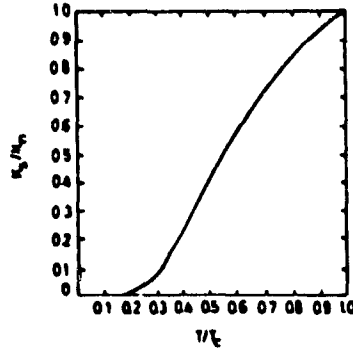


Figure 1.4: The ratio $\frac{\kappa_s}{\kappa_n}$ for the case when impurity scattering is dominant (after J. Bardeen *et al.*[10]).

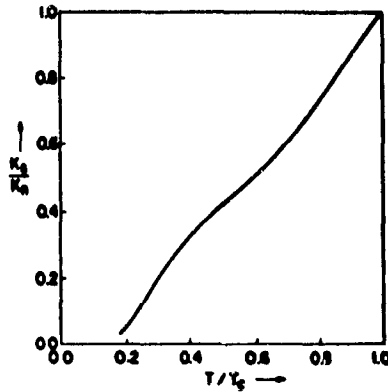


Figure 1.5: The ratio $\frac{\kappa_s}{\kappa_n}$ for the case when phonon scattering is dominant (in weak coupling limit) (after L. Tewordt [11]).

in the superconductor is shifted up by the energy gap, Δ . It is more convenient to take the ratio of the thermal conductivities of the superconductive and normal states³

$$\frac{\kappa_S}{\kappa_N} = \frac{\int_{\Delta}^{\infty} dE \cdot E^2 \frac{\partial f}{\partial E}}{\int_0^{\infty} dE \cdot E^2 \frac{\partial f}{\partial E}} \quad (1.11)$$

where f is the Fermi-Dirac distribution. This ratio is shown in figure 1.4. An attempt to use the variational method to solve the Boltzmann equation for electron-phonon scattering gave poor results but a solution by numerical methods is presented in figure 1.5.

Much below T_c (say $T \leq 0.2T_c$) the electronic thermal conductivity is small in both

³For simplicity, spherical Fermi surface is assumed.

cases since at these temperatures the number of excited electrons, i.e. the number of quasi-particles, is very small. At these temperatures the heat is carried mainly by phonons and, as shown in the previous section, $\kappa \sim T^3$.

Near T_c both contributions, κ_e and κ_{ph} , may be comparable. However the most definitive information is obtained when one of the contributions is dominant. If $\kappa_e \gg \kappa_{ph}$ the behavior of κ_e falls into two categories. When the transition temperature is on the high side of the normal state thermal conductivity maximum (obtained from equation 1.9), the thermal conductivity of the superconducting-state meets that of the normal state with quite a large angle as in figure 1.6. This is the case for lead and mercury, with low Θ_D , where the normal state thermal conductivity around T_c is dominated by strong electron-phonon scattering. The opening of a superconducting gap decreases the thermal conductivity rapidly (figure 1.5). If however the transition is on the lower side of the thermal conductivity maximum, the superconducting thermal conductivity is shifted gradually from the normal state as in figure 1.7. This is, for example, the case of indium or tin. Electron-impurity is the dominant scattering mechanism in the normal state around T_c and the thermal conductivity in the superconducting-state drops according to figure 1.4.

The most interesting case, from our point of view, is the case where κ_{ph} is comparable to κ_e . Figure 1.8 shows the thermal conductivity of NbC [14] in which a huge peak appears as the temperature drops below T_c . The peak is attributed to an increase in κ_{ph} due to a reduction in the electron-phonon scattering. A peak also appears below T_c in $YBa_2Cu_3O_{7-\delta}$, which will be discussed in section 1.3

1.2 The $YBa_2Cu_3O_{7-\delta}$ compound

It is not necessary to repeat the huge advantages and applications of the discovery of high temperature superconductors. Among the several compounds, a favorite of researchers is $YBa_2Cu_3O_{7-\delta}$ although this compound doesn't have the highest T_c . One of the reasons for this is the high sample quality that can be achieved. Most

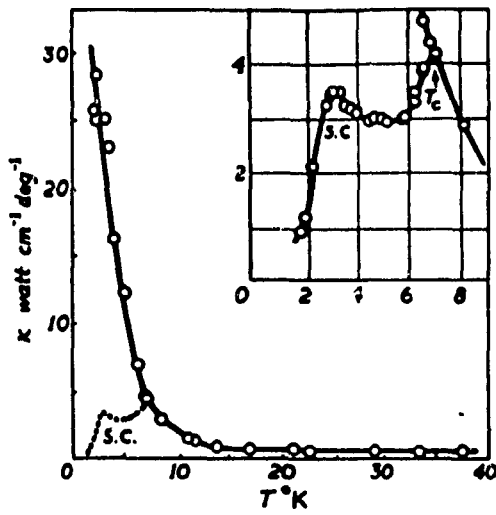


Figure 1.6: κ of lead as an example for the case in which T_c is higher than the temperature of the thermal conductivity peak (after H.M. Rosenberg [12]).

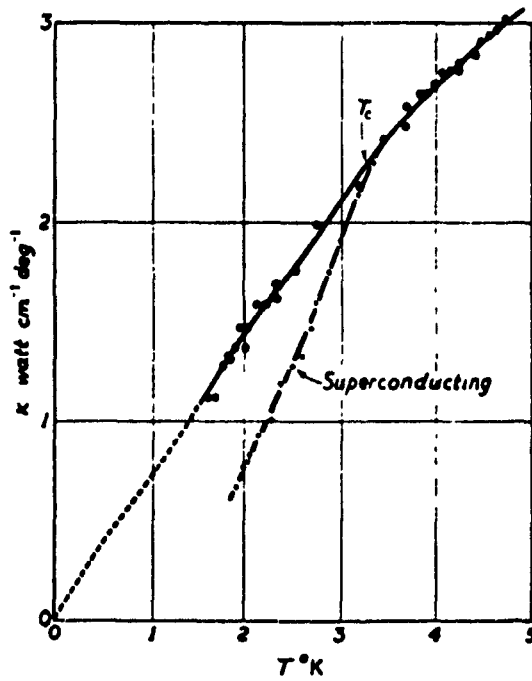


Figure 1.7: κ of indium as an example for the case in which T_c is lower than the temperature of the thermal conductivity peak (after J.K. Hulm [13]).

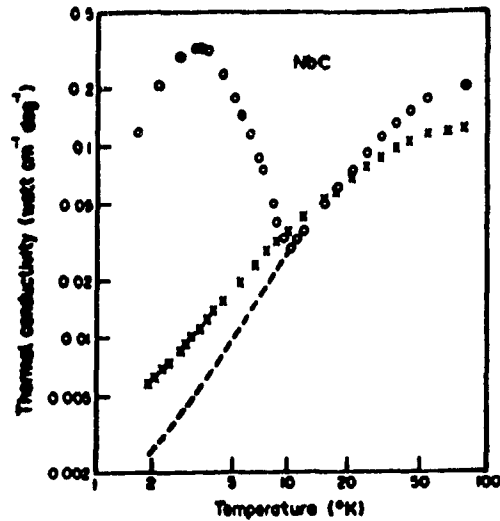


Figure 1.8: Thermal conductivity of NbC: the x curve is a non-superconducting sample; the o are superconducting samples where the dashed line is an extrapolation from the normal state of this sample (after L.G. Radosevich *et al.*[14]).

high T_c 's have different compositions and the crystal growth presents difficulties to achieve uniform one-phase samples. The $YBa_2Cu_3O_{7-\delta}$ compound makes a very good single crystal with a narrow normal-superconducting transition. The aspect of crystal growth will be discussed in the next chapter. Here I introduce the structure of the sample. Figure 1.9 shows the unit cell of the $YBa_2Cu_3O_{7-\delta}$ compound. As the other high T_c 's, all based on Cu and O , $YBa_2Cu_3O_{7-\delta}$ is characterized by CuO_2 planes in the a-b plane of tetragonal structure. The $YBa_2Cu_3O_{7-\delta}$ has a tetragonal phase (as it comes out of the furnace) with 6 oxygen atoms. After annealing, an additional O is introduced on the chain along the b axis, between two Cu atoms ($O_c(b)$ in figure 1.9) to form an orthorhombic phase. It is also important to note that the length of the b axis in the later phase is larger than the a axis only by 2% to 3%.

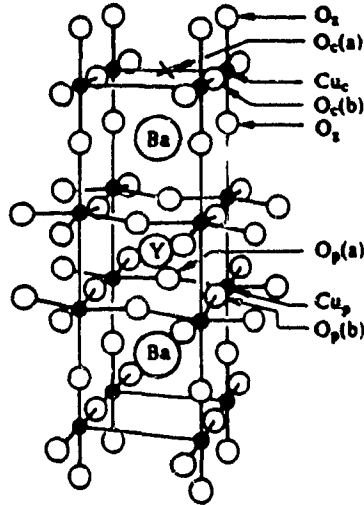


Figure 1.9: The $YBa_2Cu_3O_{7-\delta}$ unit cell (after G. Burns [15]).

1.4 Thermal conductivity of $YBa_2Cu_3O_{7-\delta}$: A review of the literature

At full oxygen doping ($\delta \approx 0$), $YBa_2Cu_3O_{7-\delta}$ is a metal. Above $T_c = 93K$, it has a fairly high resistivity. As a result, the two components of the thermal conductivity $\kappa = \kappa_e + \kappa_{ph}$, have comparable importance in the normal state and it is hard to separate between them. This issue is a major part of this section.

Several authors [17] have used thermal conductivity to study both the normal and superconducting-state of $YBa_2Cu_3O_{7-\delta}$. Those authors have found a large enhancement in the thermal conductivity as the temperature drops below T_c with a peak around 40 K, 2-2.5 times higher than its value at T_c . Particularly interesting to us are two publications that investigated detwinned single crystals. The later paper, by Yu *et al.*[18] (figure 1.10), has opened a big debate about the origin of this peak. It attributes it to the increase of κ_e , contradicting the former publication, by Cohn *et al.*[19] (figure 1.11), who claims the peak is due to phonons.

The motivation for this work was two-fold: first, to establish experimentally the correct anisotropy of κ in the a-b plane, of high quality fully detwinned $YBa_2Cu_3O_{7-\delta}$,

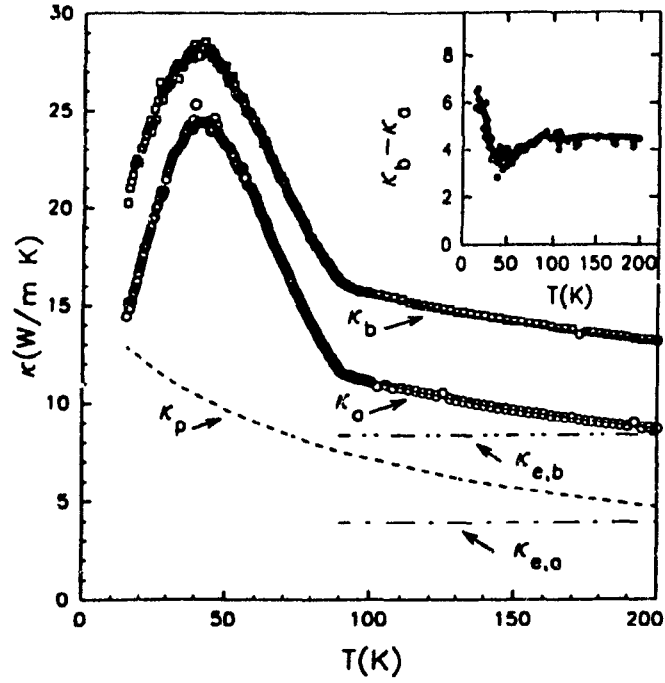


Figure 1.10: The thermal conductivity of $YBa_2Cu_3O_{7-d}$ detwinned crystal as was measured by Yu *et al.*[18].

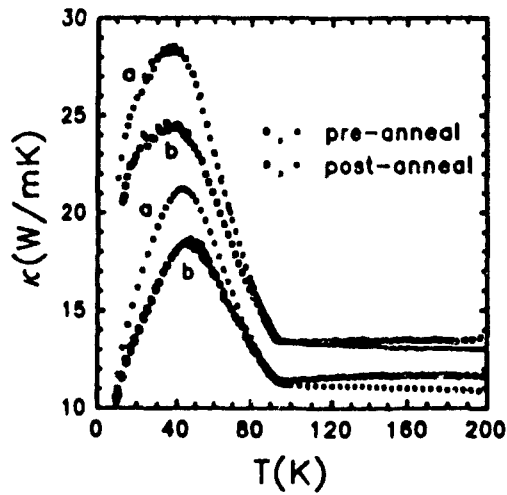


Figure 1.11: The thermal conductivity of $YBa_2Cu_3O_{7-d}$ detwinned crystal as was measured by Cohn *et al.*[19].

given the significantly different results of the two previous investigations (see figures 1.10 and 1.11). Second, to decide which of the two explanations of the peak is correct. In this section I will review those two papers (the only papers published on detwinned single crystals) commenting on the quality of samples, the experimental set-up and the analysis of the results.

Sample quality: Yu *et al.* report a relatively low value of $T_c=90.5\text{K}$ and a broad transition width of $\delta T_c \sim 1\text{K}$. They estimate resistivities of $\rho_a = 140\mu\Omega\text{cm}$ and $\rho_b = 57\mu\Omega\text{cm}$ at 200K using the Wiedemann-Franz law (assuming $L = L_0$) and find these to be in good agreement with data on samples of "similar quality"[20, 21]. However, these samples, though stated to be of similar quality, have a much higher T_c with zero-resistance of at least 92K . For comparison, our samples have (to within 15% accuracy) $\rho_a = 209\mu\Omega\text{cm}$ and $\rho_b = 100\mu\Omega\text{cm}$ at 200K . The (relatively) low T_c , the broad transition and low resistivities suggest a low annealing temperature ($\sim 450^\circ\text{C}$) with a full oxygen content of $\delta \approx 0$. However, the authors state that δ is near 0.1 which would then suggest their samples contain a fair amount of impurities (and there is an error on the real resistivities of their samples).

Cohn *et al.* grew their samples in Au crucibles. It is already established that Au crucibles contribute large amounts of impurities, mainly in the chains[22]. This will significantly reduce the a-b anisotropy in the electronic conduction.

Experimental setup: Both authors used chromel-constantan differential thermocouples to measure the temperature gradient along the sample. Yu *et al.* claim a 10% uncertainty due to the separation of differential thermocouple junctions. To this value one has to add the uncertainty due to the thickness of the samples. Since the samples are very thin ($\approx 100\mu\text{m}$), this introduces as a further uncertainty of 10%-15%. One therefore expects an overall uncertainty in the absolute value of κ of $\pm 20\text{-}25\%$. When measuring the Lorenz number this error comes in twice (for κ and for σ) hence one should aim to measure the electrical and thermal conductivity on the same sample so as to cancel out some of the geometrical uncertainties. This wasn't done by these authors but is done here.

Interpretation of results: Cohn *et al.* believe the peak in the superconducting state to be phonon dominated by measuring the electrical resistivities and employing the Wiedemann-Franz law to get an upper limit for the electronic thermal conductivity i.e. $\kappa_e \leq L_0 T / \rho$ where L_0 is the Lorenz number. By their calculation $\kappa_e / \kappa \leq 0.3-0.4$. From this value they conclude that the normal state thermal conductivity is phonon dominated.

The important scattering mechanism in this scenario is the electron-phonon process. As the temperature drops below T_c , the number of normal electrons decreases and the phonon mean free path increases, hence so is the phonon thermal conductivity, (equation 1.4), $\kappa_{ph} = \frac{1}{3} c_V c^2 \tau$.

The other paper, by Yu *et al.*, assumes the enhancement in the thermal conductivity is due to electrons by relying on conclusions from other publications[23, 25], and interpreting their own results in this way. They assume an isotropic κ_{ph} and weak electron-phonon coupling. They model κ_{ph} as $(W_0 + aT)^{-1}$ for all temperatures, where the linear term in temperature comes from the phonon-phonon scattering rate at high temperatures, $\tau^{-1} \propto T$. The term W_0 stands for phonon-electron, phonon-boundary and phonon-defect which are weakly temperature dependent and approximated as temperature independent.

To account for the superconducting state they assumed the normal state thermal conductivity $\kappa^n = \kappa_e^n + \kappa_{ph}$ where κ_{ph} remains unchanged in the superconducting state. However this formula cannot be applied at low temperatures since the phonon thermal conductivity has to drop to zero as $T \rightarrow 0$ and this is not the case in their extrapolation. The suggestion of Cohn *et al.*[26] is that at low temperatures the umklapp scattering goes as $\tau^{-1} \propto \exp(-\Theta_D/bT)$ where $\Theta_D \approx 400K$ and $b \approx 1$.

In the normal-state Yu *et al.* take the Lorenz number in the Wiedemann-Franz law as the full Sommerfeld value ($L = L_0$) so the electronic thermal conductivity of each axis in the normal state is $\kappa_e^n = L_0 \sigma T$, where σ is the electrical conductivity. They argue that since $\sigma_{a,b} \propto 1/T$, κ_e^n along each axis is temperature independent. They fit their results to $\kappa_{e,a}^n = 3.94 \pm 0.25 W/mK$ and $\kappa_{e,b}^n \approx 8.39 W/mK$. This

is inconsistent with our measurements of non-linearity of the b axis resistivity[27]. We found $\rho_b(200)/\rho_b(100) = 1.74$ (rather than 2) which implies, by the Wiedemann-Franz law, that $\kappa_{e,b}(200) = 1.15\kappa_{e,b}(100)$ so $\kappa_{e,b}$ cannot really be assumed constant. If one sets $\kappa_{e,b}(200) = 8.39 \text{ W/mK}$, one then expects $\kappa_{e,b}(100) = 7.3 \text{ W/mK}$. Such a temperature dependent is not observed.

As for the amplitude of the anisotropy, it can be attributed entirely to electrons, if $L = L_0$ (so that the deduced $\sigma_b - \sigma_a = \frac{L_0}{T}(\kappa_b - \kappa_a) = 9.32 \times 10^{-3}(\mu\Omega\text{cm})^{-1}$ and $\frac{\sigma_b}{\sigma_a} = 2.1$ are reasonable).

Yu *et al.*, with their interpretation, opened the debate about the origin of the peak in the superconducting-state, suggesting four weak points against the phononic scenario.

1. The enhancement in the thermal conductivities, κ_a and κ_b , should also show up as an enhancement in the thermal conductivity along the c axis, κ_c . But several reports consistently claimed no anomaly for κ_c below T_c [28].
2. The electronic thermal conductivity, assumed weak, was taken not to be affected or to decrease below T_c , but recent results show strong suppression of the scattering rate below T_c which should significantly increase κ_e [23].
3. It is hard to explain the anomalous properties of the normal state, e.g. the linear $\rho_a(T)$, by mainly electron-phonon scattering. However, the relative weight of the other scattering mechanisms (i.e. electron-electron, electron-spin fluctuations) is still not clear so this point is a little weak.
4. The phonon thermal conductivity has to be at least as large as the peak value in the absence of electron-phonon scattering but experiments on oxygen-deficient crystals (with no charge carriers) yield significantly smaller values. However, this argument assumes that the phonon thermal conductivity is not suppressed by introducing oxygen vacancies.

The explanation of Yu *et al.* for the enhancement in the thermal conductivity comes from the quasi-particle scattering rate. The rapid suppression in the scattering rate

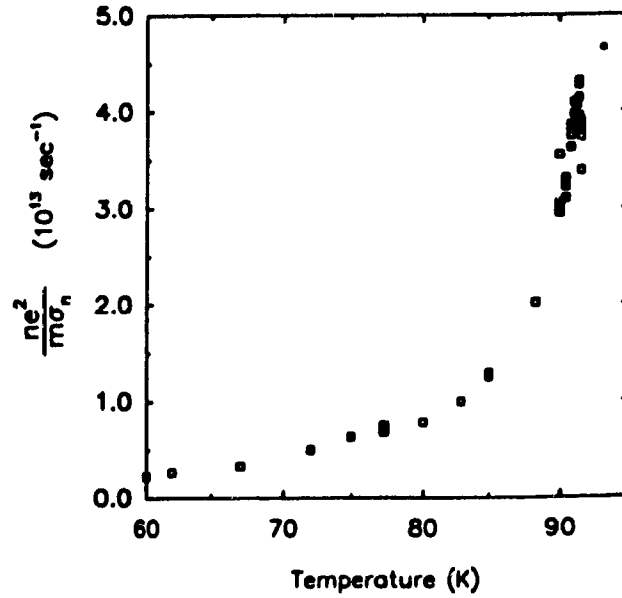


Figure 1.12: The quantity $ne^2/m\sigma_n(T)$ provides an estimate of the quasiparticle scattering rate in $YBa_2Cu_3O_{7-\delta}$ for temperatures close to T_c [25].

extracted from microwave measurements (figure 1.12) should be reflected as an enhancement in the electronic thermal conductivity (entirely due to normal electrons since Cooper pairs do not carry heat). Of course, the magnitude of such an effect will depend on the size of κ_e in the normal state and the size of $L(T)$.

Some authors find the qualitative similarity of the thermal conductivity of $YBa_2Cu_3O_{7-\delta}$ and NbC (with a huge enhancement in thermal conductivity below T_c , all due to phonons: figure 1.8) to be in favor of the phononic scenario [24]. The major difference, however, is in the dominant scattering of electrons. In NbC, electronic conduction is limited mainly by impurity scattering (this is a dirty alloy). As the temperature drops below T_c , the reduced scattering of phonons by electrons increases phonon conduction. In $YBa_2Cu_3O_{7-\delta}$ (at least in decent crystals) at temperatures around T_c , electronic conduction is limited mainly by inelastic scattering. A decrease in the electron scattering rate below T_c can arise as a result of a less efficient inelastic scattering. This could cause the electron conduction to rise if the drop in τ^{-1} is faster than the drop in the number of quasiparticle. This of course, depends on how fast and how low below T_c the scattering rate drops (in any given sample). The rise in

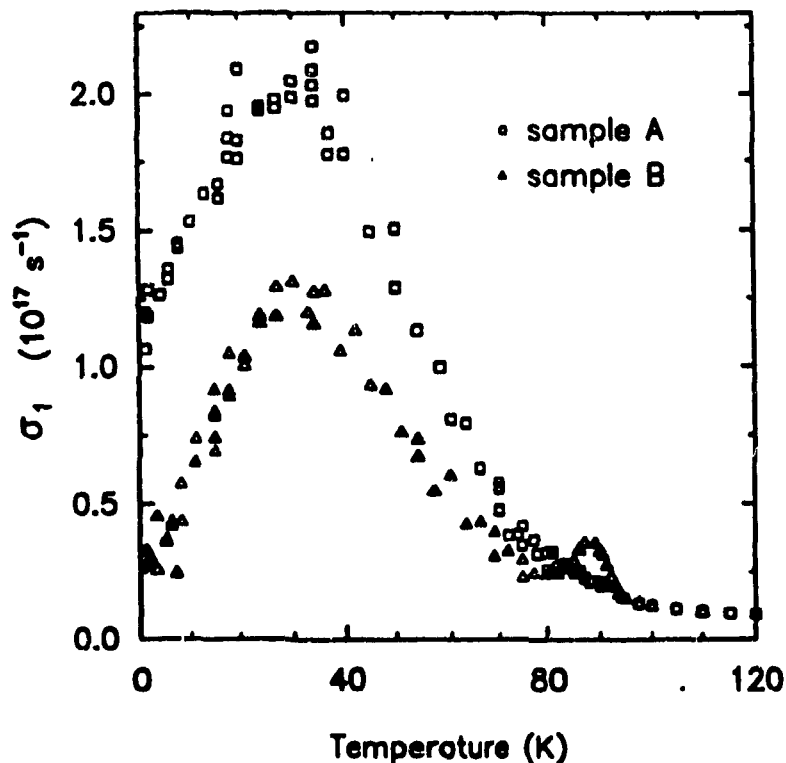


Figure 1.13: The real part of electrical conductivity extracted from microwave surface resistance [25]).

the surface resistance as the temperature drops from 77K to 35K in the microwave measurement of Bonn *et al.* (figure 1.13) is exactly this case, hence the similarity of the two curves ($YBa_2Cu_3O_{7-\delta}$, NbC) cannot account for one scenario or the other.

As for the experimental results themselves, one can see two major differences between the two papers: the first difference is the sizable normal-state anisotropy seen by Yu *et al.*, compared with the near isotropy seen by Cohn *et al.*. The second difference is at the superconducting peak where Yu *et al.* find $\kappa_b > \kappa_a$ whereas Cohn *et al.* find $\kappa_a > \kappa_b$. This striking disagreement prompted us to measure with greater accuracy the ratio $\frac{\kappa_a}{\kappa_b}$ of high quality fully detwinned crystals.

Several authors[21, 29] argue that the conductivity along the b axis proceed via two channels i.e. along the Cu-O chains and in the CuO_2 planes. In a simple model, the conductivity in the a direction is the intrinsic conductivity of the plane, the b axis conductivity is the sum of the conductivities of the a axis and the chains. In this

picture the Au doping of the chains in Cohn *et al.* may cancel out the conduction of this channel and leave an isotropy in the electrical and thermal conductivity.

Yu *et al.* interpret their anisotropy this way and find the thermal conductivity of the chains to be constant in the normal state. In the superconducting state $\kappa_b - \kappa_a$ has a shallow minimum around 40K and an enhancement below it, which features they do not attempt to explain. This will be compared and discussed with the results of this work.

Chapter 2

The Experiment

2.1 Sample Preparation

High quality $YBa_2Cu_3O_{7-\delta}$ single crystals have been grown by a self decanting flux method. The crystals have been annealed in oxygen, detwinned in a pressure cell and characterized by means of low field magnetic susceptibility, a-b plane resistivity, polarized microscope and scanning electron microscope.

2.1.1 Crystal Growth

To grow the crystals we started with two possible mixtures. The first, of Y:Ba:Cu = 1:4:10, was introduced by Rice *et al.*[30]. The other mixture of Y:Ba:Cu = 1:18:45, introduced by Wolf *et al.*[31], uses the same ratio between the Ba and Cu but a lower amount of Y since they used Ytria Stabilized Zirconia (YSZ) crucibles, part of which dissolves into the melt. A major aspect of the crystal growth is the crucible material. The commonly used crucibles are Al_2O_3 , MgO , ThO_2 and YSZ. According to Liang *et al.*[32], the Al^{+3} ions contribute large amounts of impurities by substituting for the Cu in the chain sites and the MgO crucibles give samples with low T_c since Mg^{+2} has the same charge and a similar ionic radius as Zn^{+2} , which is known to substitute for the Cu in the planes. The ThO_2 crucibles also contribute large amounts of impurities since Th^{+4} and Y^{+3} have similar radii. Liang *et al.* chose an YSZ crucible because

the Zr^{+4} has a much higher charge than the Cu atoms. We also found it to give the best results. In these crucibles we could not produce crystals from the 1:4:10 mixture but we got very good results with 1:18:45. To make the mixture we used Y_2O_3 of 99.9999% purity, $BaCO_3$ of 99.999% and CuO of 99.9999% purity. We found the purity of the materials to be a crucial aspect of the crystal growth: by using the same heating program and crucible material with $BaCO_3$ and CuO of 99.9% purity we could not even melt the mixture properly.

To extract the crystals from the flux we used the *self decantation* technique which was introduced by Gagnon *et al.*[33]. In this method a temperature gradient is applied along the crucible while crystals grow. Thermodynamically, it is favorable for the flux to move to the colder side of the crucible, leaving the crystals on the other side. The advantage of this method is that one need not turn over the crucible while it is at high temperature and several crystals are flux free. We applied a temperature gradient of about $4 - 5 \text{ } ^\circ C/cm$.

The heating program we used is a combination of those used by Liang *et al.* [32] and Vanderah *et al.*[34]:

1. Heat to $870 \text{ } ^\circ C$ in four hours. Though the furnace can reach $870 \text{ } ^\circ C$ in a much shorter time, we chose a slow heating rate to avoid a large temperature overshoot.
2. Eight hours at $870 \text{ } ^\circ C$. In this stage $BaCO_3$ decomposes into BaO for the next stage.
3. Heat in two hours to a temperature between $990 \text{ } ^\circ C$ and $1020 \text{ } ^\circ C$. This is the temperature where melting occurs. The idea is to reach the lowest temperature for chemical reaction and melting of the starting materials so as to reduce the amount of impurities due to the crucible.
4. Dwelling for 4 to 8 hours at this temperature. This stage is to ensure homogeneity of the melt.

5. Cool in one hour to 990 °C.
6. Dwell at 990°C for 5 to 20 hours. At this temperature the crystals start to grow.
7. Cooling for one hour to 950°-970 °C. In this temperature range crystals and flux coexist.
8. Cooling to 930 °C at a rate of 0.5 to 2 °C/hour. This is the self decantation stage in which flux moves to the cold side and the crystals are left in the hot side of the crucible.
9. Cooling to ambient temperature. The natural cooling rate of the furnace is low hence this stage takes about 12 hours. The low cooling rate results in surface annealing and twinning of the crystals.

When the samples are taken out of the crucible, they have an inhomogeneous oxygen content. At this stage we annealed the samples in a slow flow of pure oxygen so as to fill the chains. We heat the sample to 850 °C, for one day and then anneal for six days at 500 °C. Both LaGraff *et al.*[35] and Schleger *et al.*[36] found that at 500 °C and a pressure of 1 atmosphere, the oxygen deficiency in $YBa_2Cu_3O_{7-\delta}$ is $\delta=0.08$ to 0.1.

In order to eliminate the twinning we used a stress cell. We applied 0.5 kg along one of the edges of the sample, usually the wider one, at a temperature of 550°C (a temperature found to be a compromise between increased oxygen mobility as the temperature rises[35], and a proper function of our stress cell) for about 15 minutes (in air) and then re-annealed for one day at 500°C in oxygen.

2.1.2 Characterization

Polarized Optical Microscope

After annealing the samples one can observe twins in the a-b plane. Those twins are just alternating a and b domains due to structural transition (from tetragonal to

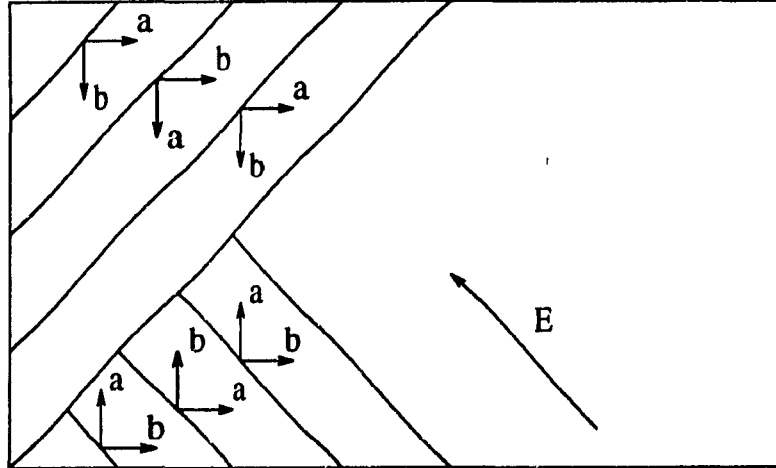


Figure 2.1: Schematic representation of twinned $YBa_2Cu_3O_{7-\delta}$ (after Gagnon *et al.*[37]).

orthorhombic, after growth, when the crystals are cooled and the surface is annealed) as in figure 2.1. In order to observe the twins and the twin boundaries we employed a polarizing microscope, in two configurations. In both cases the incident light is parallel to the c axis, so that the electric field is in the basal plane. In the first orientation the polarizer and the analyzer are perpendicular to each other and parallel to the twin boundaries, i.e. at 45° to the a or b axes. The incident light exits the polarizer at 45° to the axes. The reflected beam has electric field components r_a and r_b , and when it exits the analyzer the intensity of the light is just $I \propto |r_a - r_b|^2$. In the adjacent twin, the indices a and b are interchanged but this does not affect the intensity, so one cannot observe the different orientations of the a and b axes. Since the domain boundaries themselves have higher symmetry i.e. this configuration therefore reveals the boundaries are more isotropic, the intensity I there is much smaller. In the other configuration of the microscope, the polarizer is moved by 45° so it is parallel to one of the axes. The intensity in this case is proportional only to r_a or r_b , and one can observe different intensities for adjacent twins.

Figure 2.2 presents a picture of a small area of twinned sample when the polarizer and analyzer are in 45° to each other. Figure 2.3 presents the same zone of figure 2.3 while the polarizer and analyzer are perpendicular to each other. With this technique one can estimate what fraction of the sample is twinned, how many twin domains

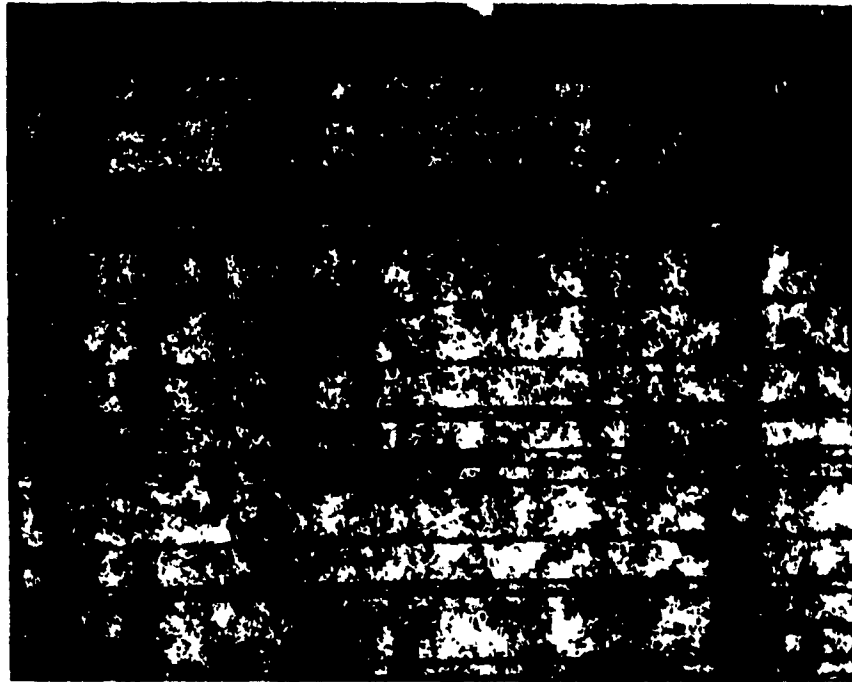


Figure 2.2: A picture of a small area of a twinned sample as it is seen in the polarised microscope when the polariser and analyser are in 45° to each other.

exist and their size. Typically, before annealing the number of twins in one orientation is about the same as in the other. After detwinning, typically about 1% of the sample is still twinned, generally in one of the corners, due to unequal stress along the side of the sample.

To look in the a-c and b-c directions we employed a scanning electron microscope. In the SEM one cannot observe the different orientations in the basal plane since the electron beam would be parallel to the c direction.

Magnetic Susceptibility

For a more quantitative characterization of the samples we employed two techniques: AC magnetic susceptibility, which is more of a volume test¹, and electrical resistivity which depends on favorable paths in the sample. The former is preferable, mainly,

¹One should note that a good surface-annealed sample (so the interior of the sample is ceramic) will result as if the whole sample is superconducting.

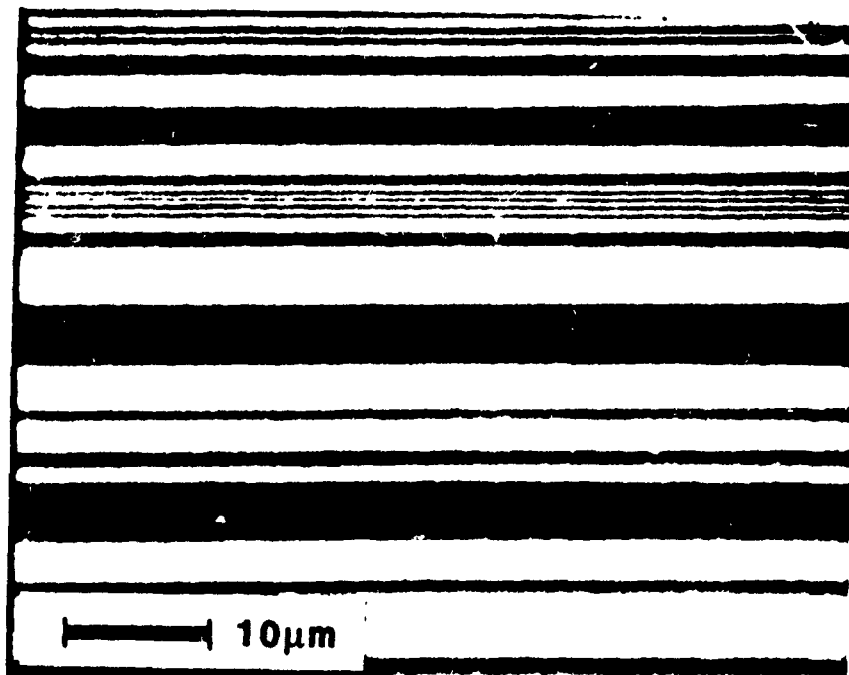


Figure 2.3: The same sone (of a twinned sample) as the previous figure with the polarizer and the analyser parallel to each other.

because it does not require any special preparation e.g. contacts.

The susceptibility apparatus is shown in figure 2.4. The probe consists of two secondary coils, 40 gauge Cu wire, 5 mm long, 6-9 mm in diameter and 1000 turns. The two coils are wound on a Teflon former in opposite directions to each other so the induced voltage in one empty coil will cancel the other as much as possible. The secondary coils are placed in the center of a primary coil, 2230 turns, 40 gauge Cu wire, 12.5 mm in diameter, and 60 mm long so as to reduce edge effects on the secondaries. We used an LR-400 resistance and mutual inductance bridge, with a maximum excitation of 10mA at 17Hz so $B_{max.} \approx 0.5\text{gauss}$. The sample was glued with insulating GE 7031 varnish to a 3mm diameter Cu rod and was placed in the center of one of the secondaries. The other side of the Cu rod is mechanically attached to the Cu tip of the probe. A platinum thermometer is mechanically attached to the other side of the Cu tip so that the heat transport between the sample and the thermometer is excellent. This apparatus dwells in low pressure of *He* gas for heat

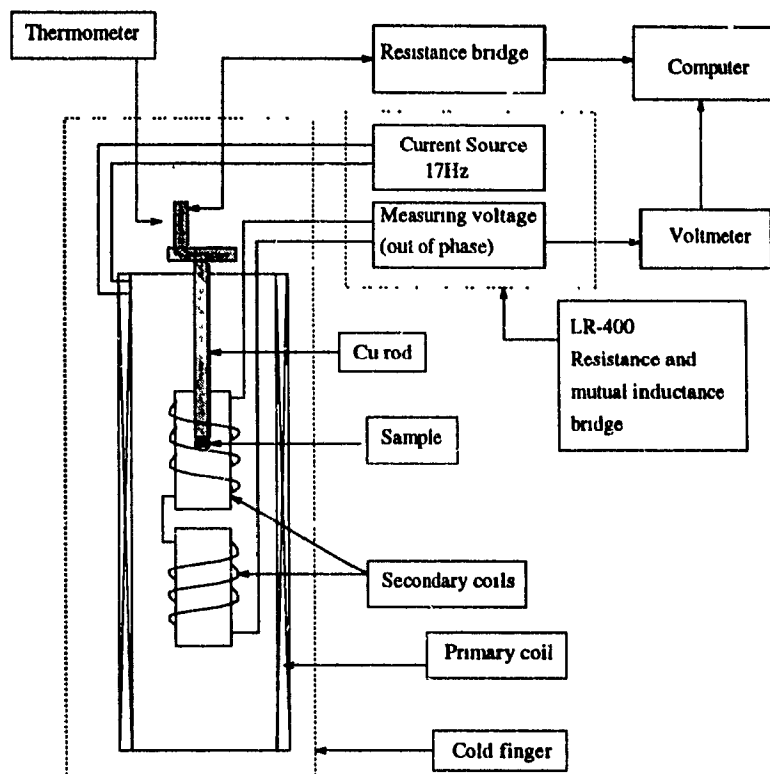


Figure 2.4: Susceptibility test

exchange between the "cold finger" and the surrounding walls so as to improve the thermal link among the several parts of the cold finger. The system is controlled by one resistance bridge for reading the thermometer and another bridge, the LR-400, in a *mutual inductance* mode to measure the susceptibility. While the sample is in the normal state, its susceptibility is negligible and one measures the difference between the secondaries (since they are not identical). A bridge offset can be applied to cancel this component. As the temperature drops below the transition point, magnetic flux is screened out of the sample and the effective volume of that secondary drops which results in a change in the total e.m.f. picked-up. In figure 2.5 one can see the transition temperature and its width. The high T_c of 93.4K and especially the very narrow transition of 0.1K (measured by 90% to 10% - top to bottom) is evidence for the high quality and homogeneity of the sample.

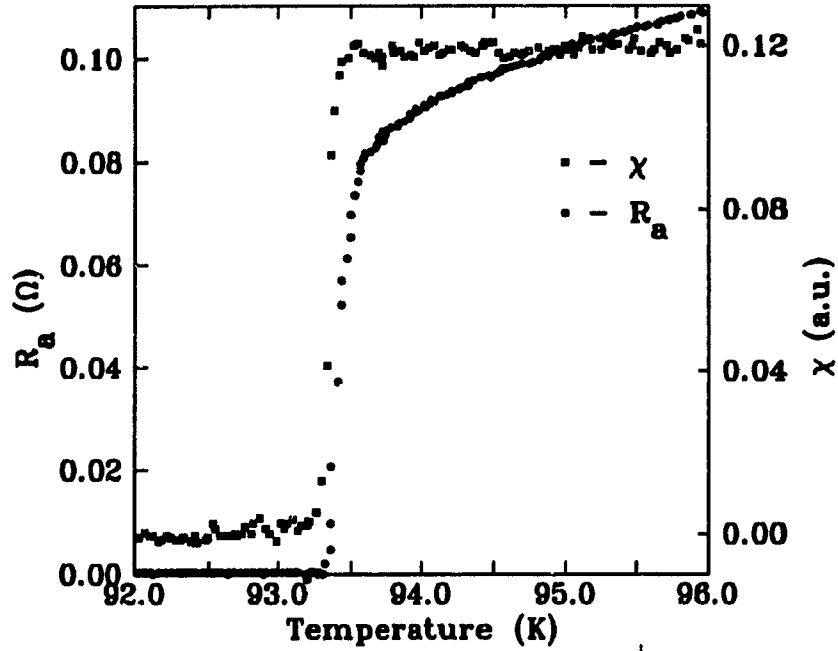


Figure 2.5: The transition temperature by resistivity (●) and susceptibility (□) test.

Electrical resistivity

As we shall see, one of the advantages of our set-up is the ability to measure the electrical resistivity *using the same contacts* as employed for the thermal conductivity. The motivation for such a design was to allow a measurement of the Lorenz number, free from geometric factor uncertainties. The electrical resistivity is also a test of the quality of the sample and its contacts. The description of the system comes later in this chapter, however, one should note that in this set-up one can measure either ρ_a or ρ_b , but not both (a curve of $\rho(T)$ will be presented in a later chapter). For a relation between the two quantities *on the same sample*, a Montgomery test was conducted in parallel with this work (R. Gagnon *et al.*[27]) and its results will be used here.

2.2 The thermal conductivity

To measure the thermal conductivity, $\kappa(T)$, we employed the steady state technique in which for every recorded point the temperature of the sample is stabilized around, say T_0 , a constant heat is applied until equilibrium is reached the temperature gradient across the sample is measured and $\kappa = \frac{\text{heat}}{\text{temperature gradient}} \times (\text{geometric factor})$ is evaluated. The targeted temperature range is 40K (the peak in the thermal conductivity in the superconducting state), and 150K for the normal state investigation. Of course, we would like to expand this range but, as will be discussed later, the thermometer limitations (at the low temperature end) and radiation losses (at the high temperature end) constrain us to this range, at least at the moment. For the purpose of this work, however, this range is satisfactory.

2.2.1 Dewar and probe

For the dewar, we used a similar set-up as for resistivity/susceptibility i.e. an external glass dewar containing the cryogenic liquids and two thin wall stainless steel tubes, one inside the other, inserted into the glass dewar as described in figure 2.6. The inner tube containing the probe needs to hold high vacuum. The area between the stainless tubes, called *the conduction chamber*, contains *He* gas at a pressure of 1 to 10^{-1} mbar, depending on the desired cooling rate.

The requirements for the probe are to hold high vacuum and to have a good thermal link to the surrounding walls. For the thermal link we used 4 BeCu strips, 5mm wide, Ω shape, attached to the Cu part of the probe (called *the cold finger*) on one side and pressed into the walls of the inner tube in the center.

Although the thermometers are far from the strips, the excellent geometric factor of the cold finger and the fact that it is solid Cu, especially between the heater and the thermometer (10mm in diameter, 30mm long) assures uniform temperature along it. This was tested by cooling down without using the heater and than warming up using the heater, against a thermometer placed in the sample area. The difference

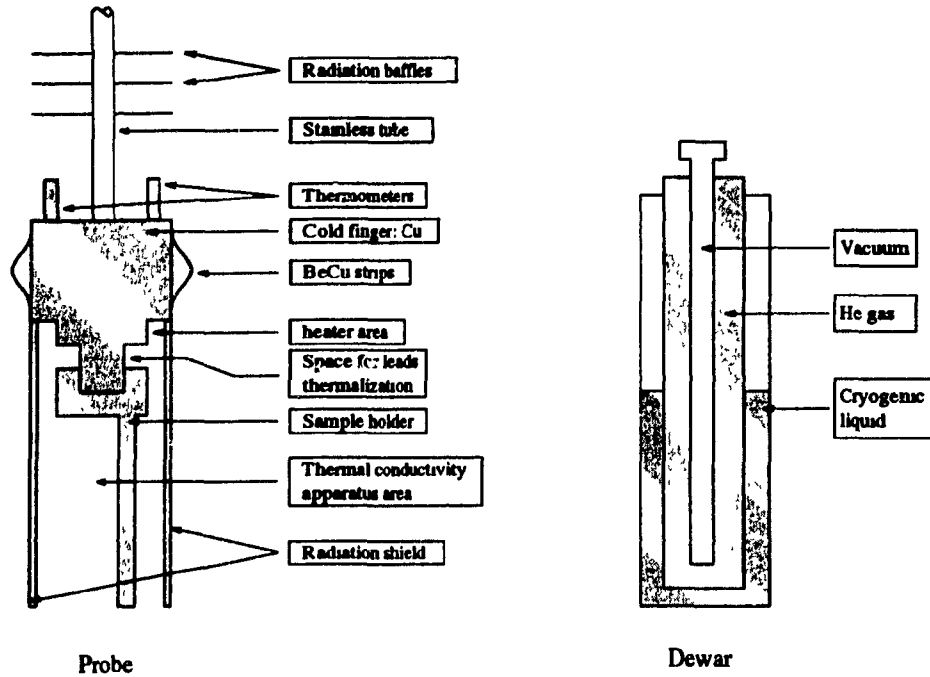


Figure 2.6: The dewar, on the right, contains liquid ${}^4\text{He}$, He gas in the conduction chamber and vacuum in the sample chamber. The shaded areas on the probe are all Cu. The space for the thermal conductivity apparatus is about 12mm high, 20mm wide and 50mm long.

was smaller than 0.5K at $T=130\text{K}$.

To reduce heat losses through radiation, a thin Cu shield was mechanically attached to the probe so the *thermal conductivity apparatus area* is surrounded by a *radiation shield* at the same temperature as the sample holder.

In order to estimate the amount of liquid ${}^4\text{He}$ boil-off due to the stainless rod and the Cu wires, we used table XIII of White [38] for the mean value of thermal conductivity of Cu and stainless steel between 300K and 4K. Using the latent heat of liquid ${}^4\text{He}$, 3 Joule/cm³, we estimated about 1.6 liter/day. This is much smaller than other loss factors, mainly through the non-perfect vacuum of the glass dewar.

2.2.2 Thermometers and heater

As will be explained later in this chapter, we required two identical resistance thermometers R_1 and R_2 , so that $\frac{dR_1}{dT} = \frac{dR_2}{dT}$ in the temperature range of the experiment, $30\text{K} < T < 150\text{K}$. Another constraint is the size of the thermometers and heater. Since the longest dimension of the sample is approximately (2mm), this should be the

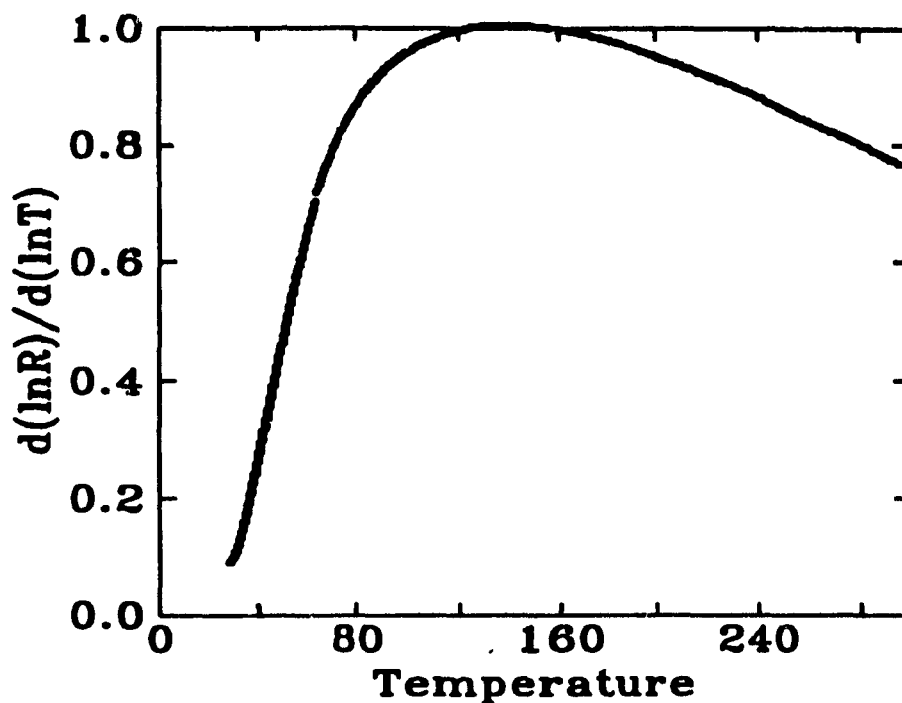


Figure 2.7: The quantity $\frac{d \ln R}{d \ln T}$ for Cu as a function of temperature as was measured by us.

size of the other parts if one requires minimal space between all parts of the thermal conductivity apparatus (to reduce heat exchange with the shield due to radiation or residual gas conduction). We started with a $2k\Omega$ carbon resistor, cut slices of 1mm thick and 3×3 mm on the surface. Silver wires were epoxied with silver epoxy or silver paste to the surface of the carbon, resulting in contact resistance of $O(200\Omega/\text{contact})$. The same process was used with silver or gold deposited on carbon surface, which reduced the contact resistance to $O(30\Omega/\text{contact})$. A bigger problem was the difference in the two thermometer resistances: $50k\Omega$ and $58k\Omega$. It was not easy to minimize that difference.

Finally we chose to make Cu thermometers. The temperature behavior of Cu is almost linear down to 77K. In fact, the important quantity, $\frac{d \ln R}{d \ln T}$, as it appears in figure 2.7, is greater than 10% for $T > 30K$. On a 7mm long, 0.5mm diameter Cu base, we wound 65cm of $12\mu\text{m}$ insulated Cu wire, as described in figure 2.8. The length of the coil itself in each thermometer is 5mm and the resistances of the two thermometers used, are 99Ω and 98Ω . On one side of the Cu base we soldered a 40

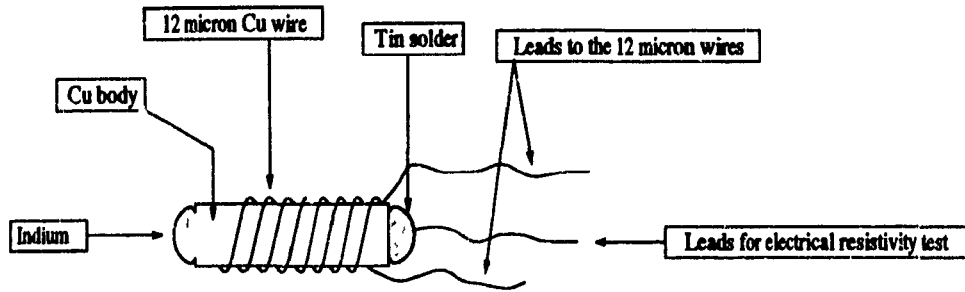


Figure 2.8: The Cu thermometer

gauge Cu wire as a lead for electrical resistivity test. On the other side we melted indium because of its low melting point so as not to burn the fragile insulation of the $12\mu\text{m}$ wire in the final assembly. With this configuration the components of the thermal conductivity apparatus make a tight "package", and also enable us to measure the electrical resistance of the sample together with the thermal conductivity.

The same principle guided the design of the heater, replacing the Cu wire by $25\mu\text{m}$, 100cm long manganin wire which gave $929\ \Omega$ at room temperature.

2.2.3 Thermal conductivity apparatus

Physical circuit

The technique used to measure thermal conductivity is a 4 probe method which requires a cold point, a heater and two thermometers in between. To the sample we silver-epoxied four $100\mu\text{m}$ silver wires as described in figure 2.9. The characteristic distance along the Ag wires between the sample and the other components is 2mm. The manganin coils thermally isolate the thermometers and heater from the Cu base. To estimate the heat leak through these coils, from table I of White [38], the thermal conductivity of manganin at 150K is $13\text{Wm}^{-1}\text{K}^{-1}$. With $25\mu\text{m}$ diameter and 4cm long, the thermal leak of each component (i.e. 5 coils) is $1\mu\text{WK}^{-1}$. For our sample, $l=2\text{mm}$ and $s = 1.1 \times 0.09\text{mm}^2$, the thermal conductance is $250\mu\text{WK}^{-1}$. With such a ratio the heat loss through these coils is negligible compared with the heat flow through the sample. This is even more true at lower temperatures.

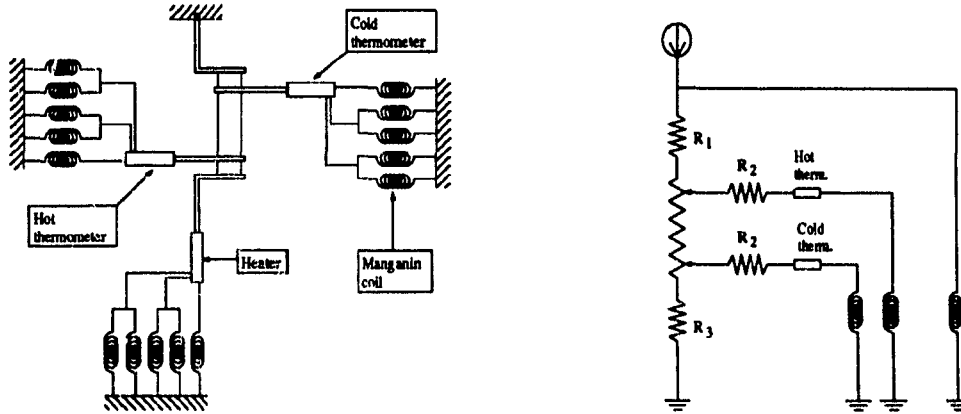


Figure 2.9: A detailed drawing of the thermal conductivity apparatus is shown on the left. Ag wires are epoxied along the sample, perpendicular to the direction of current. The manganin coils are connected to the electrical leads of the probe. On the right, an electric analog with power as current source, and temperature as potential, is shown. The little resistors, R_1 , stand for contact resistances. The one between the heater and the sample, R_1 , is the most significant resistor since it includes the manganin insulation in the heater. It was found experimentally to be three times the sample resistance. R_2 , much smaller than R_1 , has no thermal or electrical significance. R_3 has an excellent mechanical contact hence even smaller than R_2 .

The losses through radiation were more significant. Experimentally we found that by supplying the heater with a power of 0.25mW , its temperature increases by $5 - 5.5^\circ\text{C}$ (more or less at any temperature), a value which was obtained using the measured temperature dependence of manganin resistance. Assuming an emissivity factor $\epsilon=1$ for all surfaces, the heat lost by the heater per second

$$\dot{Q} = \sigma A [(T + 5)^4 - T^4] \simeq 4\sigma AT^3 \times 5$$

where $\sigma = 5.67 \cdot 10^{-12} \text{W/cm}^2 \text{K}^4$ and A is the surface of the heater. Thus $\dot{Q}_{loss} \approx 0.12\text{mW}$ at 150K . This value was found to be consistent with our measurements of the Lorenz number of silver (which we measured for calibration of the system, see next section) in which we found $L > L_0$ at $T > 150\text{K}$. At this point we surrounded the thermometers and heater with aluminized mylar and shortened the length of Ag wires. Since the emissivity factor of Al, $\epsilon \simeq 0.1$ [38], \dot{Q}_{loss} becomes less than 5% of the supplied power. After these improvements we obtained satisfactory results up to 150K .

Another mechanism for heat loss is the heat exchange through the residual gas in the cryostat. Since the pressure in the sample area is lower than 10^{-5}torr (actually 10^{-6}torr for high temperatures and 10^{-7}torr below 78K) we could rely on the fact

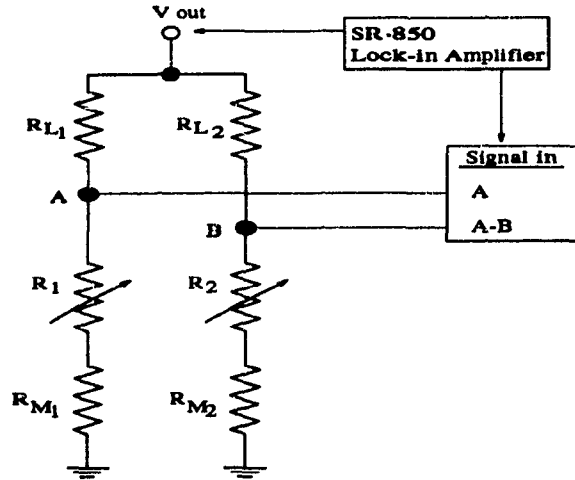


Figure 2.10: The electrical circuit of the experiment. $R_{L1,2}$ are limiting resistors of $10\text{k}\Omega \pm 1\%$. $R_{1,2}$ are thermometers and $R_{M1,2}$ are manganin coils.

that the mean free path of the gas molecules is larger than the distance between the thermal conductivity apparatus and the radiation shield and employ equation 48 of ref. [38]

$$\dot{Q} = 0.016a_0 p_{mm} (T_2 - T_1), \quad a_0 \leq 1$$

where p_{mm} is the pressure in mm of Hg, \dot{Q} is in $\frac{\text{W}}{\text{cm}^2}$ and $\Delta T_{\text{Heater}} = T_2 - T_1 \approx 5$. a_0 , called the accommodation coefficient, is smaller than one. Using the heater surface area, $\dot{Q} = 0.25 \mu\text{W}$ (for $a_0 = 1$), which is also a negligible effect.

The electrical circuit

The electrical circuit of the thermal conductivity apparatus is described in figure 2.10. Before turning to the mathematics we make several approximations:

1. $R_{L1} = R_{L2} \equiv R_L \gg R_1, R_2$. The limiting resistors R_L are thin film $10\text{k}\Omega \pm 1\%$. In fact we found $10.02\text{k}\Omega$ and $10.01\text{k}\Omega$ respectively. The resistance of the thermometers and manganin coils are less than 1% of R_L throughout the temperature range of this experiment.
2. Although the resistance of the manganin coils, R_M , is temperature dependent (and we make use of it later) it is negligible compared with Cu, i.e. $\frac{dR_M}{dT} \ll \frac{dR_{1,2}}{dT}$.

This fact was confirmed at the lowest value of $\frac{dR_{1,2}}{dT}$ in this experiment, i.e. at 30K we measured $R_{1,2}$ (4 probe measurement) and compared $\frac{dR_1}{dT}$ with $\frac{d(R_1+R_M)}{dT}$.

3. For a small temperature change, ΔT , the change in the thermometer resistances is

$$\Delta R = R(T + \Delta T) - R(T) \simeq \frac{dR}{dT} \Delta T$$

The validity of this linear approximation, in particular at low temperatures will be discussed later.

The potential at point A or B is

$$V_{A,B}(T) = \frac{V_0(R_i + R_{M_i})}{R_L + R_i + R_{M_i}} \simeq \frac{V_0}{R_L}(R_i + R_{M_i}), \quad i = 1, 2$$

where V_0 is the voltage generated by the Lock-in Amplifier. $V_{A,B}$ can be measured as a function of temperature and one obtains a calibration

$$\frac{dV_{A,B}}{dT} = \frac{V_0}{R_L} \left(\frac{dR_i}{dT} + \frac{dR_{M_i}}{dT} \right) \simeq \frac{V_0}{R_L} \frac{dR_i}{dT}$$

In fact, within the 1% uncertainty, $\frac{dR_1}{dT} = \frac{dR_2}{dT}$ so $\frac{dV_A}{dT}$ is the calibration for both thermometers which we will call simply $\left(\frac{dV}{dT}\right)_{\text{calibrated}}$.

Next, we apply a small temperature gradient at a constant cold finger temperature which causes the potential at say, point A, to increase by ΔV_A . Mathematically

$$\begin{aligned} \Delta V_A &= V_A(T+\Delta T) - V_A(T) = \frac{V_0}{R_L} [R_i(T + \Delta T) - R_i(T) + R_M(T + \Delta T') - R_M(T')] = \\ &= \frac{V_0}{R_L} \left(\frac{dR_i}{dT} \Delta T + \frac{dR_M}{dT} \Delta T' \right) \simeq \frac{V_0}{R_L} \frac{dR_i}{dT} \Delta T \end{aligned}$$

where $T + \Delta T'$ is some average temperature on the manganin coil between the sample and the cold finger. Under approximation 2, we ignore the manganin contribution, hence

$$\Delta T = \frac{(\Delta V_A)_{\text{measured}}}{\left(\frac{dV}{dT}\right)_{\text{calibrated}}}$$

The same treatment can be made for the difference in the potentials $V_A - V_B \equiv V_{A-B}$:

$$\begin{aligned} \Delta V_{A-B} &= [V_A(T + \Delta T_A) - V_B(T + \Delta T_B)] - [V_A(T) - V_B(T)] \simeq \\ &\simeq \left(\frac{dV}{dT} \right)_{\text{calibrated}} (\Delta T_A - \Delta T_B) \end{aligned}$$

which is just $T_A - T_B$ while the sample has a temperature gradient i.e. if $\Delta T_A = T_A - T_0$ and $\Delta T_B = T_B - T_0$:

$$\Delta T_A - \Delta T_B = T_A - T_B = \frac{\Delta V_{A-B}}{\left(\frac{dV}{dT} \right)_{\text{calibrated}}} \quad (2.1)$$

One should note that we make use of the same $\left(\frac{dV}{dT} \right)_{\text{calibrated}}$ for both thermometers due to the similarity of the resistances. This assumption will be shown later, in page 43, to be justified.

2.3 Test of Ag sample

At an early stage of the experiment we had the need to test the apparatus. For this reason we chose to measure a well known material. We used a 100 μ m Ag wire, 14mm long, from the same material as for the leads to the sample (from the manufacturer: 99.997% purity). The distance between the thermometers is 11mm so that the thermal conductance is of the same order as for our YBCO samples, $\simeq 0.3 \times 10^{-3} W/K$. The manufacturer data gives $\rho_{Ag} = 1.586 \mu\Omega cm$. The measured sample resistance at room temperature, $R = 23.3 \pm 0.1 m\Omega$, deviates from the calculated one, $R = 22.21 m\Omega$, by 5% due to geometric factor uncertainty.

Figure 2.11 presents the electrical resistance of the sample at low temperatures. The "steps" reflect the accuracy of the last digit on the resistance bridge, and introduce an error of 5% at 80K to 11% at 40K.

We measured the thermal conductivity of the Ag sample at several points between 40K and 170K. At higher temperatures we found the heat loss due to radiation to be significant as was mentioned earlier (and as a result we later added radiation shields to all the components of the thermal conductivity apparatus and minimized the length

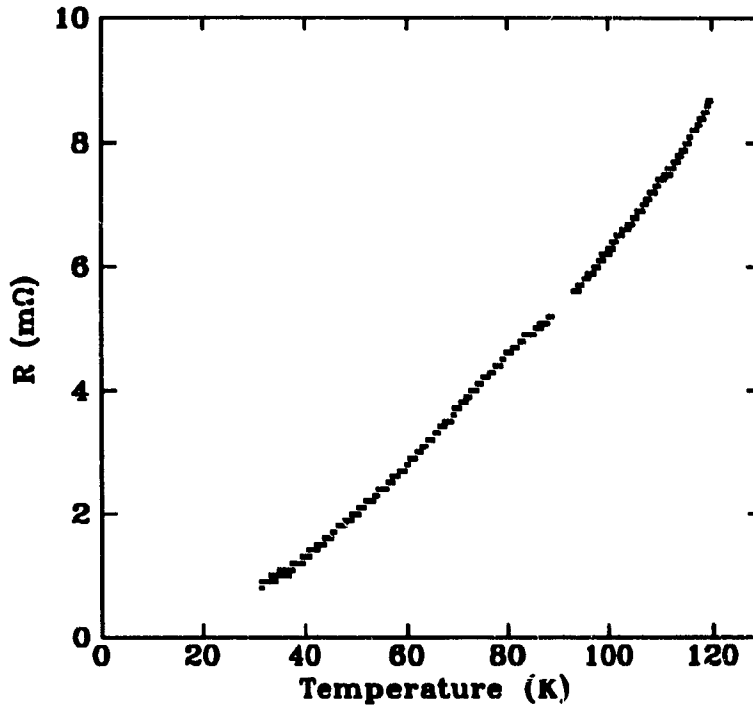


Figure 2.11: The measured electrical resistivity of the Ag sample. The distance between adjacent "steps" is just the last digit on the lowest scale of the resistance bridge.

of the Ag wires between the $YBa_2Cu_3O_{7-\delta}$ sample and the Cu thermometers, for the following experiments). The measured Lorenz number is presented in figure 2.12. Although the error due to the electrical resistance data is large (especially at the lower temperatures), the measured Lorenz number is in rough agreement with the expectations. For comparison, figure 2.12 presents published values for the Lorenz number of Ag of 6N purity[3]. The higher values of our sample can be explained by the different impurity concentration as was discussed earlier (figure 1.2).

As a result of this experiment we limited our measurements in $YBa_2Cu_3O_{7-\delta}$ to temperatures lower than 150K (because in Ag, $\kappa \leq L_0\sigma T$ in this temperature range).

Furthermore, we estimate that the improvements implemented for $YBa_2Cu_3O_{7-\delta}$ have reduced heat losses by radiation by at least a factor of 10 at 150K.

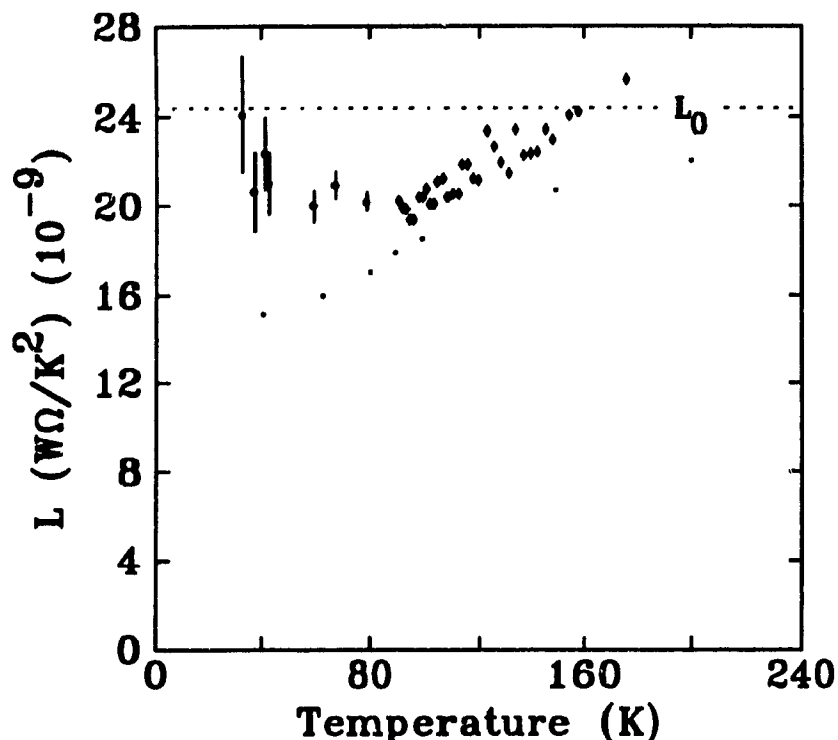


Figure 2.12: Lorenz number as was measured by us (o, ◇) before correcting for radiation, and as was measured by others (□) for samples of higher purity. Error bars are due to the "steps" of the previous figure.

2.4 Experimental procedures

Four samples have been measured: two detwinned crystals, one with $J \parallel a$ (labeled A) and the other with $J \parallel b$ (B), a twinned sample (C) and a deoxygenated sample (D) with $O_{7-\delta}$ of $\delta = 0.7$. In all cases we started measurements by cooling while measuring the sample electrical resistance, the heater resistance, the potential across one thermometer (including the manganin coil) and the difference in the voltage across each thermometer, ΔV . This enabled us to obtain a curve for $R_{sample}(T)$, $V_{therm.}(T)$, and hence also dV/dT and $R_{heater}(T)$. Once the temperature was stabilized at 90K or 30K we measured the time response of the thermal conductivity apparatus to reach equilibrium, and estimated it for all temperatures. The final step was to increase the temperature in steps and recording the heater power and ΔV to get $\kappa(T)$.

1. Since the cooling rate was kept low, no significant temperature gradient was found between the sample and the Pt/Ge thermometers (the probe temperature). This was confirmed during the thermal conductivity experiment when

V of hot thermometer (mVolts)

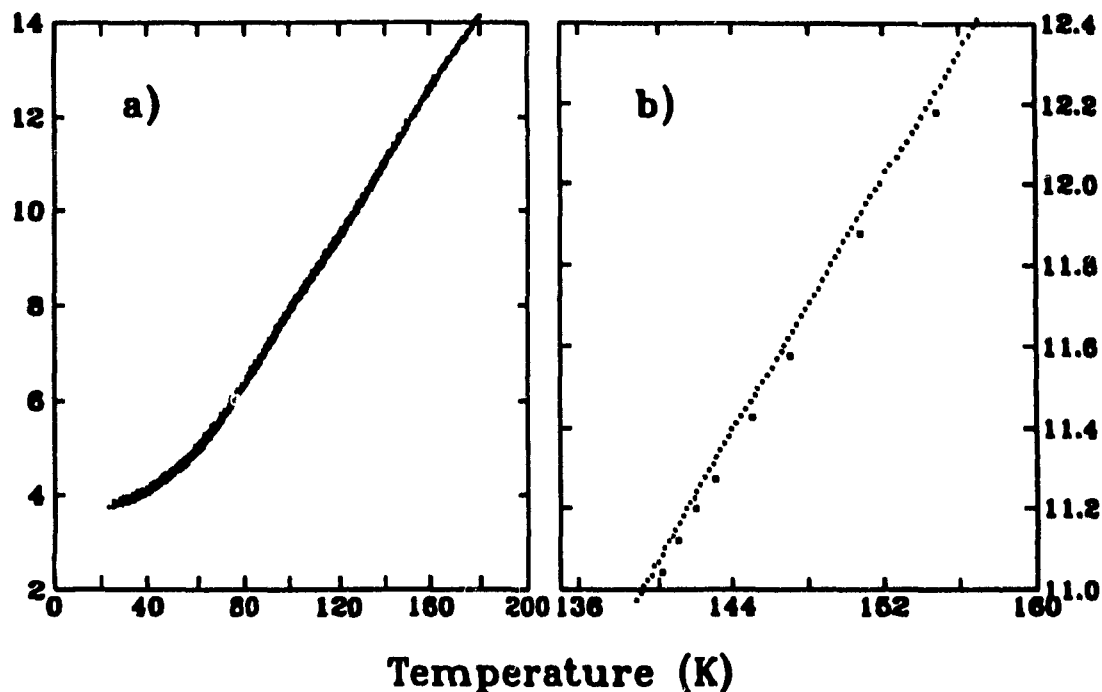


Figure 2.13: a) The Cu thermometer vs. probe temperature (obtained from Ge/Pt thermometer) while cooling down (circles) and while heating (squares). b) A magnification of the temperature range with the most significant deviation.

heat was applied to the probe (to stabilize its temperature) and the resistance of the Cu thermometers was compared to the resistance obtained while cooling down. The results are shown in figure 2.13, which reveal a maximum deviation of 0.5%, at 160K.

2. The electrical resistance of the samples is presented in figure 2.14. δT_c , the width of the transition, for the superconducting samples, 90% to 10% top to bottom, is 0.1K. The resistivity of sample A (the sample with $J \parallel a$), ρ_a , is calculated using the measured geometric factor: $l = 1.3mm$, $s = 1.1mm \times 0.09mm$. We estimate the uncertainty on the geometric factor to be 10% to 15%. Now, the anisotropy of the electrical resistivity was carefully measured by Gagnon *et al.*[27]: For nominally identical crystals it is $\rho_a/\rho_b = 2.15 \pm 0.05$ at 250K. Dividing this ratio by the ratio of resistances R_a/R_b at 250K results in the ratio between the geometric factors to within $\sim 3\%$ uncertainty (instead of $2 \times 10 - 15\%$). The

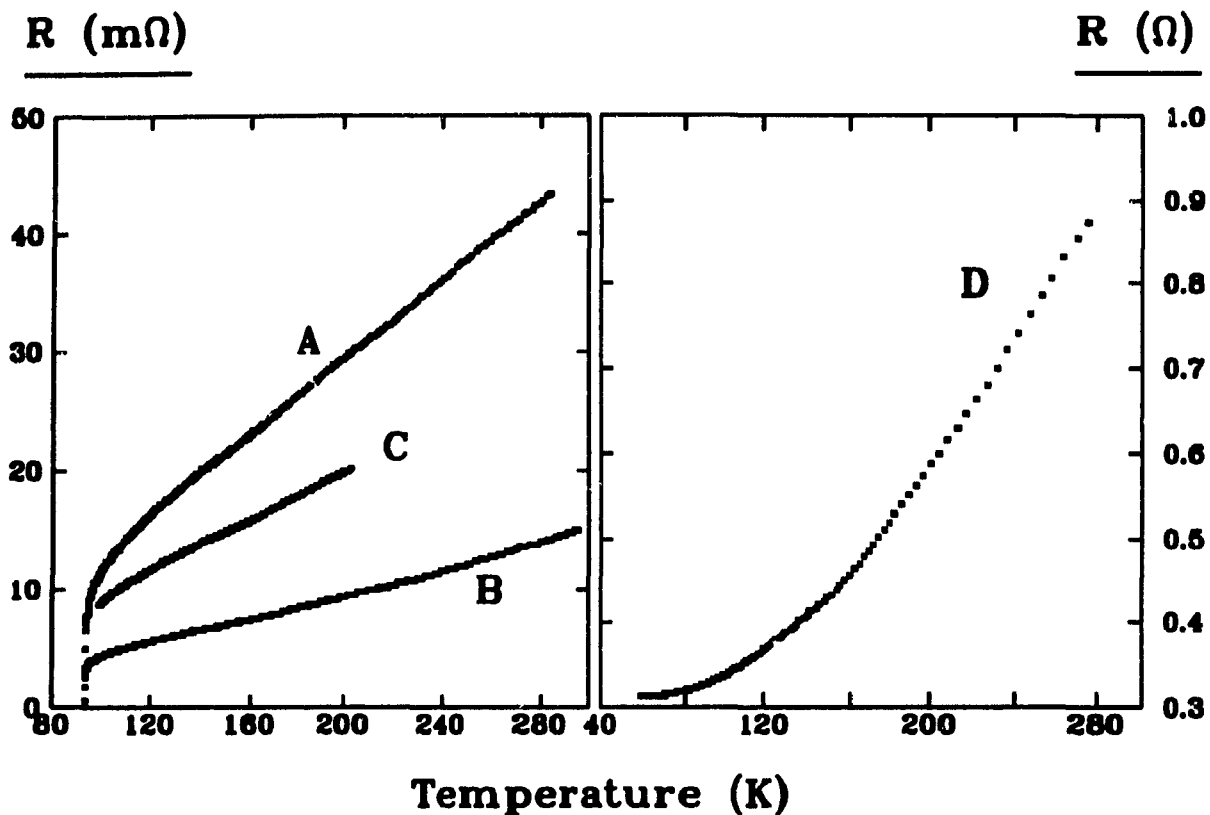


Figure 2.14: Measured electrical resistance of the superconducting samples, on the left, and of the deoxygenated sample, on the right. All samples have comparable geometric factors. Sample A: $J||a$; sample B: $J||b$; sample C: twinned; sample D: deoxygenated.

same procedure was used for the twinned sample for which the resistivity work gave $\rho_{twinned} = \frac{1}{2}(\rho_a + \rho_b)$ [27]. The uncertainty for the deoxygenated sample is the usual 10% to 15%.

3. To measure thermal conductivity in the steady state one should stabilize the temperature of the probe. We required the temperature controller to be stabilized to the last digit e.g. at 150K the fluctuations are of order $\frac{\Delta R}{R} = \frac{0.01\Omega}{50.66\Omega}$, which results in $\Delta T \leq 0.025K$.
4. Once the temperature of the probe is stable, the period, from the time heat is applied on the sample till the whole apparatus reaches equilibrium, is temperature dependent due to the dependence of the heat capacity and thermal conductivity. Figure 2.15 presents the time dependence at 90K of the voltage difference between the two thermometers, V_{A-B} , for $J||b$, showing equilibrium is reached

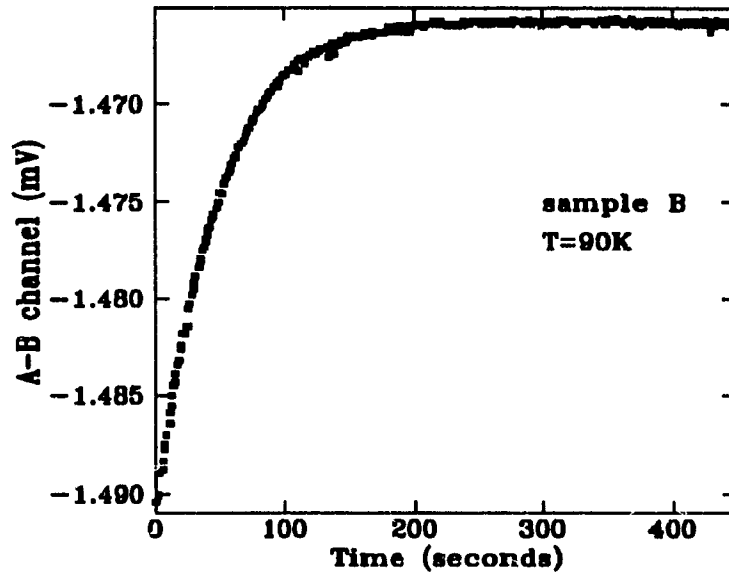


Figure 2.15: Time response of A-B channel at 90K of sample B with applied heater current of 0.866mA (Power=0.66mW).

after 4-5 minutes. The same was done at 30K and we found $\tau(30K) \simeq 30sec$. Next, we estimated $\tau(T)$ by linear extrapolation between $\tau(30K) = 1min.$ and $\tau(90K) = 7min.$ to ensure equilibrium has been reached at all temperatures.

5. For each point taken, the system records: 1) the difference potential for the pair of thermometers (and its standard deviation²) before ($V_{A-B}^{Q=0}$) and after (V_{A-B}^Q) heat is applied, 2) the heater voltage (V_{Heater}) while being heated with constant current (I), and 3) the probe temperature (T_{Probe}) as obtained from a calibrated Ge (or Pt) thermometer.
6. Using the measured curve of $V(T)$ for the Cu thermometer without heat (shown in figure 2.13), we obtain the temperature of that thermometer while heated.

²It is one of the features of the LIA SR-850, to record values for a certain time (we chose 10sec.) and return mean value and deviation from it, for both A and A-B channels. This enabled us to identify bad points due to noise, instrument errors etc.

From the curve fit of $\frac{dV}{dT}(T)$ we calculate³ $\frac{dV}{dT}(T_{hot\ thermometer})$. From equation 2.1:

$$\Delta T = [V_{(A-B)_{with\ heat}} - V_{(A-B)_{without\ heat}}] / \left(\frac{dV}{dT}\right)_{T_{hot\ thermometer}} \quad (2.2)$$

and the thermal conductivity $\kappa = \frac{I \cdot V_{heater}}{\Delta T} \times (\text{geometric factor})$.

At very low temperatures, $\frac{dV}{dT}$ changes quickly, hence it does not have the same value for the hot thermometer as for the cold one and equation 2.2 needs corrections.

Defining T_Q to be the temperature at the middle point between the thermometers while the temperature gradient ΔT is applied, the potential across each thermometer, e.g. the hot one, is

$$V_A \left(T_Q + \frac{\Delta T}{2}\right) = V_A(T_Q) + \left(\frac{dV_A}{dT}\right)_{T_Q} \frac{\Delta T}{2} + \frac{1}{2!} \left(\frac{d^2V_A}{dT^2}\right)_{T_Q} \left(\frac{\Delta T}{2}\right)^2 + \dots \quad (2.3)$$

V_A is temperature dependent but $V_{(A-B)_{without\ heat}}$ was found experimentally to be constant to within the noise (see figure 2.16), so $\frac{d^n V_A}{dT^n}(T) = \frac{d^n V_B}{dT^n}(T)$. Writing equation 2.3 for $V_B \left(T_Q - \frac{\Delta T}{2}\right)$, the measured voltage difference, $V_A - V_B$ with heat, can be written

$$\begin{aligned} V_A \left(T_Q + \frac{\Delta T}{2}\right) - V_B \left(T_Q - \frac{\Delta T}{2}\right) &= V_A(T_Q) - V_B(T_Q) + \\ &+ 2 \cdot \left(\frac{dV}{dT}\right)_{T_Q} \cdot \frac{\Delta T}{2} + \frac{2}{3!} \left(\frac{d^3V}{dT^3}\right)_{T_Q} \left(\frac{\Delta T}{2}\right)^3 + \dots \end{aligned} \quad (2.4)$$

Since $V_A(T) - V_B(T)$ is constant, the top part of equation 2.4 is just $V_{(A-B)_{with\ heat}}$ on the LHS and $V_{(A-B)_{without\ heat}}$ on the RHS where

$$V_{(A-B)_{with\ heat}} - V_{(A-B)_{without\ heat}} \equiv \Delta V_{A-B}$$

To fit $V_A(T)$ we used a polynomial of fourth order for the range $30K < T < 80K$:

$$V_A(T) = 2.814 \cdot 10^{-3} + 8.837 \cdot 10^{-5}T - 2.968 \cdot 10^{-6}T^2 + 5.032 \cdot 10^{-8}T^3 - 2.5045 \cdot 10^{-10}T^4$$

³The hot thermometer and cold thermometer refer to the one closer to the heater and the one closer to the base, respectively.

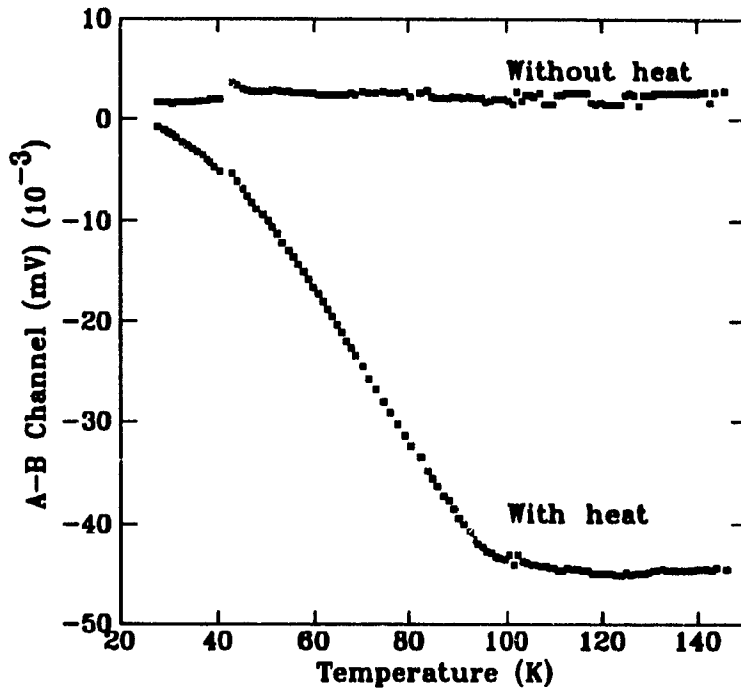


Figure 2.16: The Voltage difference between the two thermometers, channel A-B of the LIA, before and after applying heat.

and a linear fit from 80K to 150K : $V_A(T) = 5.1684 \cdot 10^{-5} + 7.8666 \cdot 10^{-5}T$. The deviation of the measured values from the fit, $\frac{\Delta V}{V} = \left| \frac{V_{\text{measured}} - V_{\text{fit}}}{V_{\text{measured}}} \right| \leq 0.7\%$ over the entire range. To within this accuracy, equation 2.4 has no higher orders than the cubic term. Rewriting equation 2.4

$$\Delta T = \Delta V_{A-B} \left(\frac{dV}{dT} \right)_{T_Q}^{-1} - \left[\frac{2}{3!} \left(\frac{d^3V}{dT^3} \right)_{T_Q} \left(\frac{dV}{dT} \right)_{T_Q}^{-1} \left(\frac{\Delta T}{2} \right)^3 \right] \quad (2.5)$$

where the last term in equation 2.5 is a correction to the linear expression. For $T_Q = 30K$ and a characteristic $\Delta T \leq 1K$, this correction term is smaller than 0.26mK, much smaller than the accuracy of the fit i.e. equation 2.2 is not really an approximation in our case, but essentially the correct equation. This is still subject to the approximations of page 35 however.

Since T_Q is not known, we start with $\frac{dV}{dT}(T_{\text{hot thermometer}})$ to find ΔT so $T_{\text{cold}} = T_{\text{hot}} - \Delta T$. Employing new $\frac{dV}{dT}(T_{\text{cold thermometer}})$, we find a new, recursive, ΔT which converges after a few iterations. Just after the first iteration, however, the error on ΔT at $T=30K$ and $T=40K$ are 10% and 3% respectively i.e for $T > 40K$ this is

within the general uncertainty.

The range $30K < T < 40K$, however, suffers from another problem due to the much decreased sensitivity of the Cu thermometers. For a little noise of $\sim 0.25\mu V$ in V_{A-B} , the noise on ΔT is about $\frac{2 \times 0.25}{\frac{dV}{dT}}$. Since $\frac{dV}{dT}(40K) = 29\mu V K^{-1}$ and $\frac{dV}{dT}(30K) = 11\mu V K^{-1}$, the noise on ΔT is 0.017K and 0.05K respectively. For a ΔT of 0.5K, this is noise at the level of 3.5% and 9% (for $T = 40K$ and $T = 30K$, respectively). We see that 30K is really the lowest temperature this set-up can reliably access.

As for other possible corrections:

1. The current through the Cu thermometers was 0.1mA so the power generated by self heating varies from about $1\mu W$ at ambient temperature to about $0.2\mu W$ at 30K whereas a characteristic heater current was 0.5mA with $R_{Heater} \approx 900\Omega$ hence self heating corrections are less than 0.4%.
2. The thermal leak through the manganin coils was less than 1% at temperatures smaller than 150K (page 33).
3. The corrections due to the temperature dependence of the manganin coils (since we measure the potential across both the Cu thermometer and one manganin coil) was found to be less than 5% at 30K, and to drop rapidly as the temperature increased (page 36).
4. The major uncertainty comes from heat loss due to radiation. In page 34, we found it to be less than 5% at $T=150K$ (and dropping rapidly as the temperature decreases).

As a result, apart from geometrical factor considerations, the uncertainty at all temperatures on the absolute value of the thermal conductivity is kept under 3%, with a slight increase at the edges of the temperature range. One should note, however that these corrections affect all curves in the same way.

Chapter 3

Results and Discussion

3.1 Results

Figure 3.1 presents the thermal conductivity of all four samples. Before discussing the results, a few details. The six (isolated) points for the deoxygenated sample at low temperatures were measured manually. At that stage the liquid He was finished (before the dewar was cold enough to condense the injected He) so we recorded the values manually, calculating the temperature drift (of the hot thermometer), and as a result, the error on $\frac{dV}{dT}$ due to the drift. For sample B we lost 2 points at 43K because a transfer of liquid He froze a rubber seal. All points above 40K are subject to error of 3-4%. Below 40K the error becomes increasingly significant and the results should not be taken too seriously. Although our geometric factor uncertainty is 10-15%, the ratio of κ for the different superconducting samples is much smaller since it relies on the anisotropy of the electrical resistivity, and this was determined to within 3% [27].

3.2 Discussion

Let us discuss first the *a* axis results.

Using the measured resistance (fig 2.14) we estimate the Lorenz number $L = \frac{\kappa\rho}{T}$. Since we used the same contacts for both electrical and thermal conductivity,

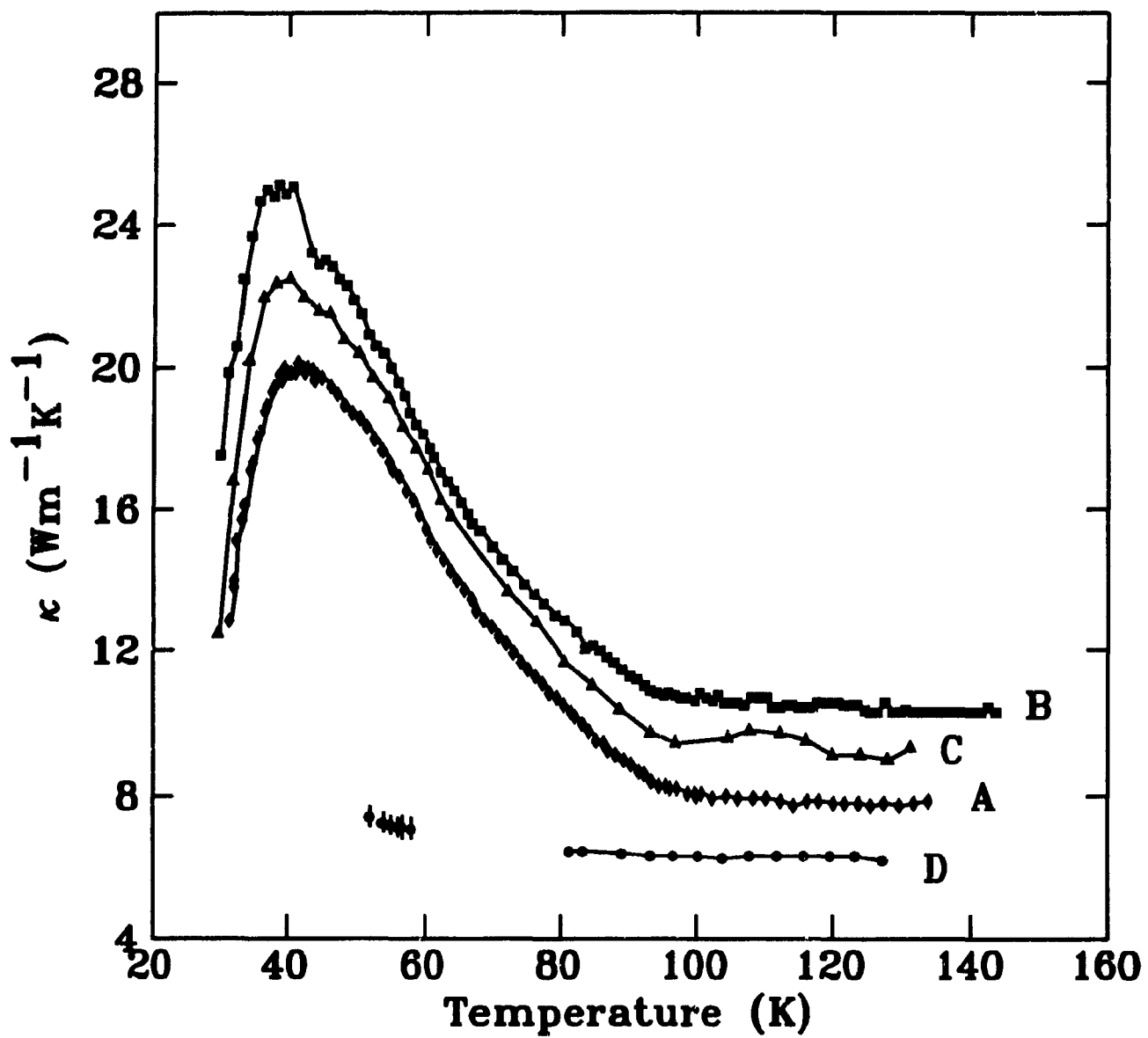


Figure 3.1: Thermal conductivity of all samples: A(\diamond , $J||a$), B(\square , $J||b$), C(Δ , twinned), D(\circ , deoxygenated).

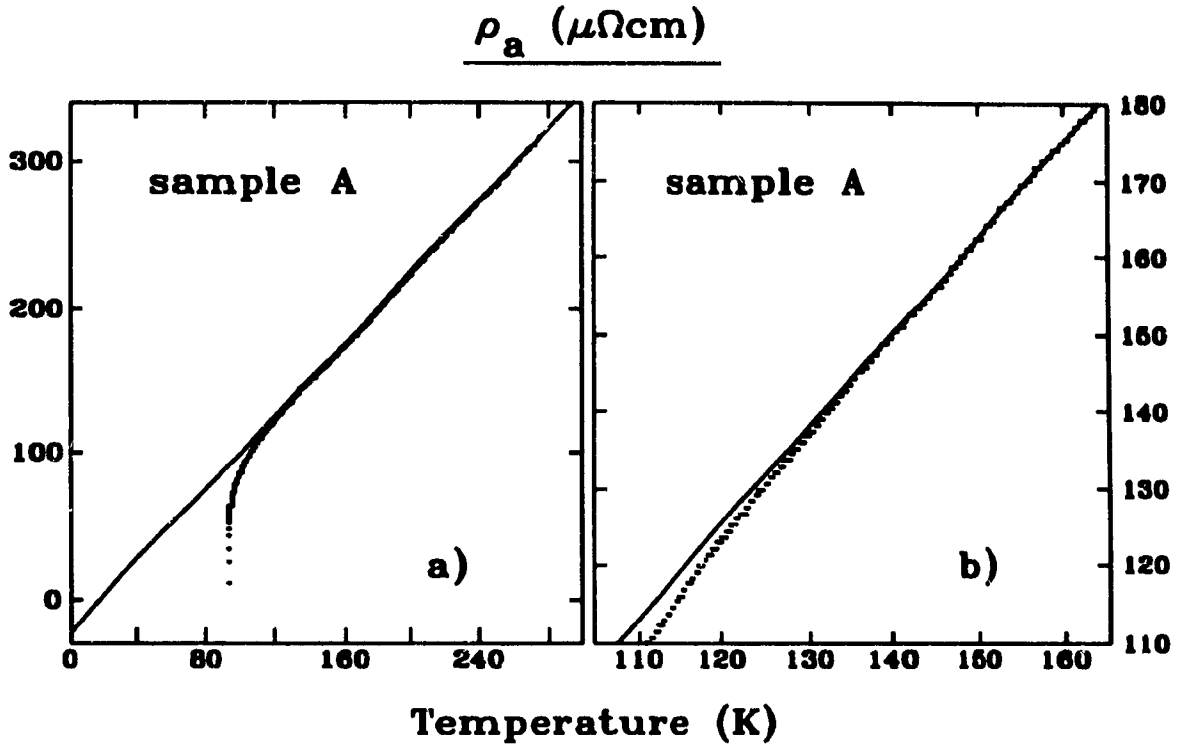


Figure 3.2: Measured ρ_a for sample A: a) with a linear fit above 140K; and b) zooming in the temperatures in which superconducting fluctuations start. The solid line is a linear extrapolation of high temperature data.

the geometric factor cancels out. Figure 3.2 presents the resistivity of the a axis using the dimensions of sample A: $l=1.3\text{mm}$ (distance between thermometers) $s=1.1 \times 0.09\text{mm}^2$. The normal state can be linearly fit to $\rho_a = -23.16 + 1.24T(\mu\Omega\text{cm})$ where the temperature T is in Kelvin. This is in agreement with the results of Gagnon *et al.*[27]. The deviation from the linear fit at temperatures above 140K is smaller than the accuracy of the bridge with which we measured the resistance. As the temperature drops toward T_c , the resistivity of the sample decreases faster due to superconducting fluctuations (an issue currently being investigated).

Figure 3.3 presents the Lorenz number for the a axis. As the temperature drops toward T_c , the resistance decreases faster than the linear behavior (figure 3.2: superconducting fluctuations) which causes a rapid decrease of L_a near T_c . For reasons of radiation corrections we couldn't measure reliably the thermal conductivity at temperatures higher than the fluctuation regime. If we calculate the Lorenz number using

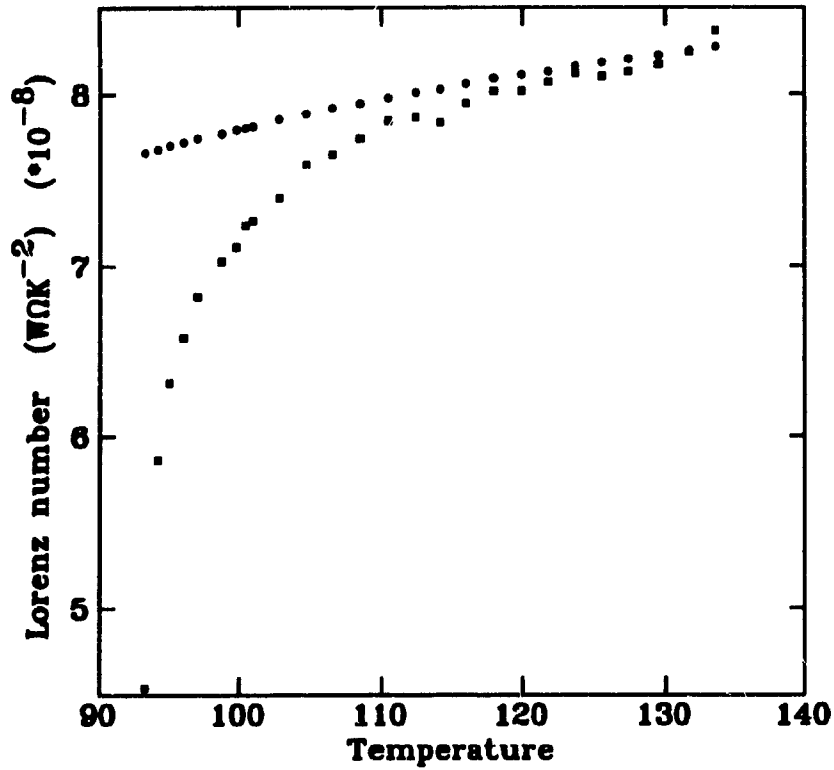


Figure 3.3: The Lorenz number of the a axis, $L_a = \frac{\kappa_a \rho_a}{T}$, using the resistivity curve: (□) and the linear fit to the resistivity curve (○), as in the previous figure.

the linear fit of figure 3.2, we find that $L_a = 8 \times 10^{-8} W\Omega K^{-2}$ around 120K, with a small temperature dependence. One should note, however, that this dependence is within the experimental uncertainty (radiation, residual gas, etc.). Since the Lorenz number of the electrons cannot be greater than $L_0 = 2.44 \times 10^{-8} W\Omega K^{-2}$, the phonon contribution to the a axis thermal conductivity is at least $\frac{L_a - L_0}{L_a} \approx 70\%$ of κ_a .

The Lorenz number of the deoxygenated sample (D) is about $70L_0$, so that the electronic contribution to the conduction is negligible compared to the phonon conduction. Since we didn't reach temperatures low enough with the deoxygenated sample, I cannot present a resistivity graph that includes the transition temperature. This was measured at a later time and we found a T_c of about 30K.

As was mentioned earlier, several authors believe that the conduction in the b direction proceeds via two channels: the $Cu-O$ chains and the CuO_2 planes where the latter is given by the conduction of the a axis. If one assumes the phonon conduction is isotropic, $\kappa_b - \kappa_a$ is electronic only. This assumption is based on the fact that

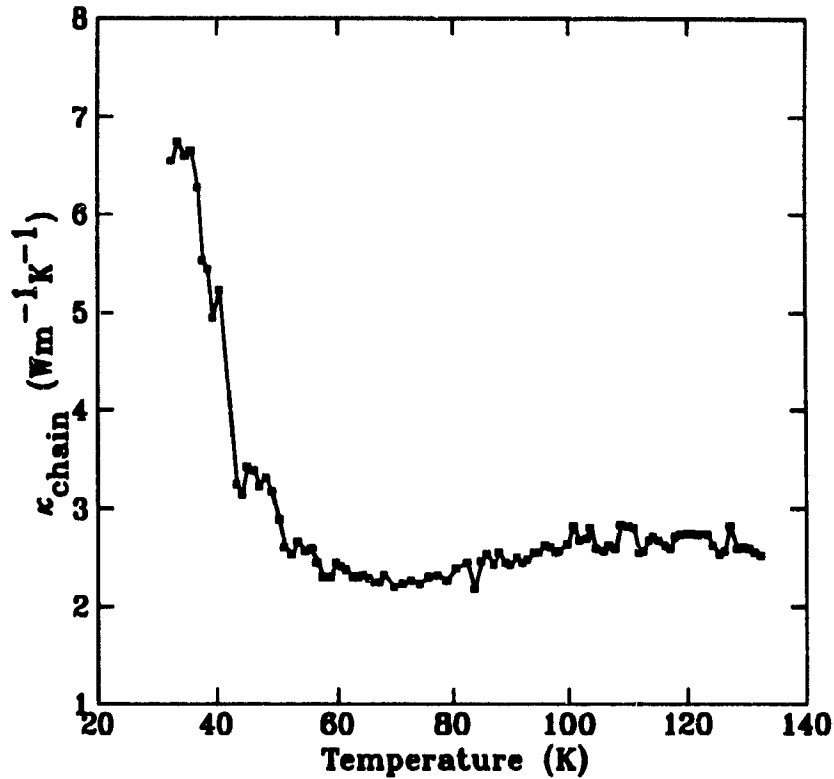


Figure 3.4: $\kappa_b - \kappa_a$ as a function of temperature.

the $YBa_2Cu_3O_{7-\delta}$ structure is only slightly away from tetragonal symmetry, so that one can expect the sound velocity to be virtually the same along a and along b. In this case the difference between κ_a and κ_b may be attributed entirely to electronic conduction along the chains.

Under these assumption, the thermal conductivity of the chains $\kappa_{ch} = \kappa_b - \kappa_a$ is shown in fig 3.4. The normal state thermal conductivity, is temperature independent and $\kappa_{ch} = 2.7 \pm 0.12 Wm^{-1}K^{-1}$. As the temperature drops below T_c , the chain conduction has a shallow minimum (similar to Yu *et al.* but smaller), with an increase as the temperature drops further. No clear anomaly at T_c is observed, like in κ_a or κ_b taken separately.

At temperatures below 40K ($\kappa_{ch} \approx 5 Wm^{-1}K^{-1}$), the huge peak comes from the precise shape of the curves of $\kappa_{a,b}$. With the enlarged error below 40K, the magnitude and exact location (on the temperature scale) of the peak is somewhat questionable, so the results at these low temperatures should not be taken too seriously. Clearly,

an experiment tailored for this range is needed.

The electrical resistivity of the chains, $\rho_{ch} = \frac{1}{1/\rho_b - 1/\rho_a}$, fit $\rho_{ch} = 85.637 + 0.00252T^2$ $\mu\Omega cm$, where T is in Kelvin and $\frac{R_{measured} - R_{fit}}{R_{fit}} \approx 2\%$ due to instrument error (the "steps" in figure 3.2). The Lorenz number of the chains, $L_{ch} = \frac{\kappa_{ch}\rho_{ch}}{T}$, varies from $L_{ch}(100) = 2.51 \pm 0.16 W m^{-1} K^{-1}$ to $L_{ch}(150) = 2.56 \pm 0.16 W m^{-1} K^{-1}$. If the chain conduction is only electronic, the Lorenz number, to within the experimental error, takes its full Sommerfeld value, L_0 . It should be mentioned here that the value of κ_{ch} was obtained from two different samples. Since those samples were prepared under identical conditions, it is believed that the chain conduction is identical for both samples. Absolute value of κ_a adjusted to yield correct ratio ρ_a/ρ_b (to determine the geometric factors ratio).

From the work on electrical conductivity[27], it was found that electrons are not scattered by twin boundaries since $\rho_{ab} \approx \frac{1}{2}(\rho_a + \rho_b)$. Similarly, for the thermal conductivity of a twinned sample, if twin boundaries do not scatter heat carriers, then one expects $\kappa_{twinned} \approx \frac{1}{\frac{1}{2}(1/\kappa_a + 1/\kappa_b)}$. Since we find $\kappa_{ab} \approx \frac{1}{2}(\kappa_a + \kappa_b)$ we can conclude that phonons, also, are not strongly scattered by twin boundaries.

As part of a collaboration with Prof. K. Behnia, of Orsay, France, the thermal conductivity of samples A and B was measured in a dilution refrigerator at temperatures down to 0.1K. Figures 3.5 and 3.6 present κ/T vs. T and T^2 at low temperatures as measured by K. Behnia and L. Taillefer in Orsay, on the same samples as used by us for higher temperatures. The isotropy of the T^2 term in figure 3.5 (observed for $0.4K < T < 0.6K$, and probably due to electron-phonon processes) and the T^3 term in figure 3.6 (observed below about 0.35K, probably due to phonon-boundary scattering) implies that phonon velocities are isotropic. Although at much smaller temperatures, this supports the assumption of isotropic κ_{ph} near T_c . From fig 3.6, at very low temperature there is a finite linear term in addition to the phonon T^3

¹Since κ_{ch} is constant but ρ_{ch} is not proportional to T, the Lorenz number should have a temperature dependence. Although this dependence is very small, much smaller than the error in our case, this is what we pointed out as a weak point in the interpretation of Yu *et al.* (page 18).

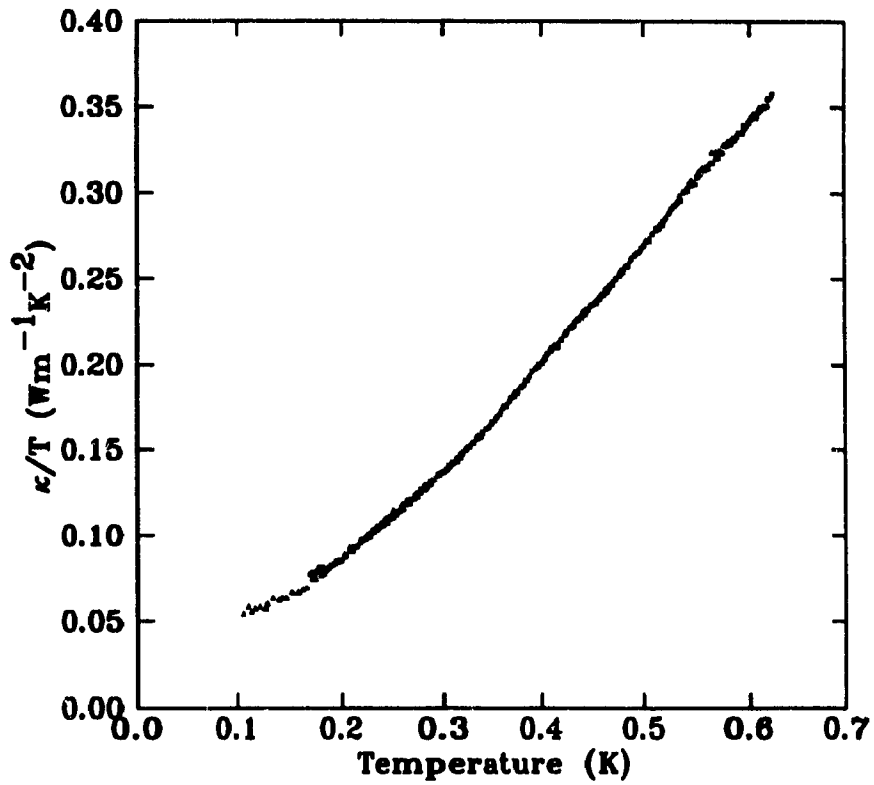


Figure 3.5: κ/T as a function of temperature in the a (\square) and b (\triangle) axes.

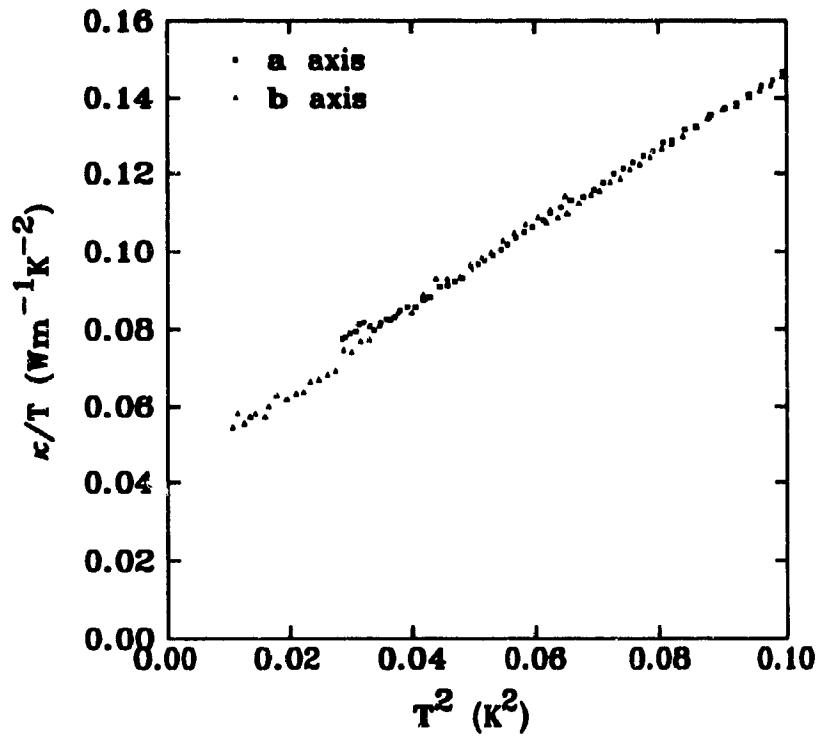


Figure 3.6: κ/T as a function of T^2 in the a (\square) and b (\triangle) axes.

term. A linear term is normally associated with electrons scattered by impurities. Since the actual value of κ/T is also isotropic (to within $\sim 3\%$), this implies isotropic electronic conduction. κ_{chain} , in this case, is very small if not zero. The measured value of $\sim 0.4mWK^{-2}cm^{-1}$ is close to the value of κ_e/T at T_c : if one accepts that $L_e = L_0$, then $\kappa_e/T \simeq \frac{L_0}{100} = 0.25mWK^{-2}cm^{-1}$. This means that the product $n_e\tau$ is comparable for $T \rightarrow 0$ and $T = T_c$. From microwave measurements by Bonn *et al.*[39], $\tau(T \rightarrow 0) \approx 100\tau(T_c)$ in good crystals. Hence the number of (uncondensed) electrons, $n_e(T \rightarrow 0)$, is about 1% of the number of electrons at T_c .

The isotropy at low temperatures suggests that the heat is carried by the electrons in the plane and the chains are shorted out. One explanation for this is that $\tau_{chain} \ll \tau_{plane}$, as one would extrapolate from the normal state resistivity (i.e. $(\rho_0)_{plane} \ll (\rho_0)_{chain}$). This is apparently in contradiction to the results of σ_1 data (in microwave measurements by Zhang *et al.*[41]) where a factor 2 anisotropy is obtained at all temperatures above 1K. The data on σ_1 , however, did not go below 1K.

The existence of finite number of uncondensed electrons as $T \rightarrow 0$ was already suggested by Bredl *et al.*[40], however the isotropy in our results contradicts their interpretation in which these electrons are in the chains.

Another question under a debate these days, is what kind of superconductor is $YBa_2Cu_3O_{7-\delta}$ i.e. whether it is an s-wave or something more exotic. Finite number of electrons at $T \rightarrow 0$ may, in fact, argue for gap with zeros, e.g. d-wave.

3.3 Conclusions

This work had two main aims:

1. Since the only two published works on detwinned crystals have such different results (figures 1.10 and 1.11: anisotropy vs. isotropy of the normal state, κ_b bigger vs. smaller than κ_a in the superconducting state), we measured two high quality detwinned crystals, and imposed a smaller uncertainty on the ratio κ_b/κ_a ($\sim 3\%$ rather than 20%).

Our samples appear to be of a higher quality than those of the others. We used thermometers instead of a thermocouple so we were able to measure both electrical and thermal conductivity on the same contacts and hence determine the Lorenz value accurately.

2. To decide between the two scenarios for the peak of the thermal conductivity in the superconducting state. After reviewing the arguments of the previous authors, on the one hand Yu *et al.* who claim this peak is due to enhanced electron conduction, and on the other hand Cohn *et al.* who attribute it to enhanced phonon conduction, we could not a priori, decide in favor of one of them.

Our approach was to study the effect of deoxygenation on the thermal conduction to help separate the phonon and electron contributions. To this end we compared high quality crystals, prepared under identical conditions, with different oxygen doping ($\delta=0.1$ and 0.7).

A first result, using the electrical resistivity results of Gagnon *et al.*, was that phonons, as electrons, are not scattered by twin boundaries.

Under the assumption that the phonon conduction is isotropic, so that all anisotropy is electronic only, we found that the Lorenz number, in the range 100 to 140K, take its full Sommerfeld value, L_0 . This would suggest that the inelastic scattering of electrons (at least in the normal state) is probably not due to phonons which would normally give a reduced L at $T = \Theta_D/4$.

From the previous section, the phonon contribution to the thermal conductivity of the superconducting samples, assumed isotropic, is about $\frac{L_a - L_0}{L_a} \kappa_a = 5.4 W m^{-1} K^{-1}$, nearly 70% of κ_a . For the deoxygenated sample, (where $\frac{\mu_p}{T} \simeq 70 L_0$ at $T=100K$, hence assumed entirely phonon dominated) $\kappa_{deox} = 6.35 W m^{-1} K^{-1}$, nearly temperature independent, with 10% uncertainty due to geometric factors. This is very close to the thermal conductivity due to phonons along the a axis. If deoxygenation of the sample does not result in a sizable increase in phonon scattering due to oxygen vacancies, the near equality of the two numbers implies that the electrons and phonons

are weakly coupled. In other words, if electrons and phonons are not coupled, then deoxygenation (hence removing the electronic contribution) leaves the phonon contribution unchanged. In this picture, the enhancement in the superconducting state would be due to electrons since fig 3.1 shows that the phonon conduction, down to the thermal conductivity peak at 40K, remains almost unchanged from its value in the normal state.

This conclusion is invalid, however, if the increased number of oxygen vacancies results in a decrease of κ_{ph} combined with, and nearly compensated by, an increase due to weaker electron-phonon scattering, thus supporting the strong electron-phonon coupling case. Again, if one assumes strong coupling, deoxygenation reduces the phonon conduction but at the same time the amount of electron-phonon scattering decreases, and with our results of the normal state, the two processes nearly compensate each other. As the temperature drops below T_c , the amount of electron-phonon scattering decreases dramatically and κ increases as was previously suggested by Cohn *et al.* to explain the peak.

In the low temperature regime, we found that some electrons remain normal even as $T \rightarrow 0$ however we concluded that these electrons are in the planes and not in the chains, contrary to what had been previously proposed [40].

Qualitatively, we found that our thermal conductivity results are similar to those of Yu *et al.*. As for the interpretations of the results, we cannot conclude from the thermal conductivity alone which of the scenarios is better. However, in favor of the electronic scenario:

1. $\kappa_b - \kappa_a$ is given very closely by $L_0T(\sigma_b - \sigma_a)$. This implies that an important fraction of heat in the normal state is carried by electrons (about 30% and 45% for the a and b axes, respectively).
2. $\kappa = 6.4 \pm 1Wm^{-1}K^{-1}$ in the deoxygenated sample is very close to $\kappa_{ph} = \kappa_a - L_0T\sigma_a = 5.5 \pm 0.9Wm^{-1}K^{-1}$ in well oxygenated sample. This suggests a weak electron-phonon scattering (at least plausible).

3. Assuming $L = L_0$ at all temperatures, the curve of κ_e/T looks a lot like the peak in $\sigma_1(\omega)$ versus T (figure 1.13): a) it has the same position, about 40K, and b) same height i.e. $\frac{\kappa_e}{T}(\text{peak}) \simeq 20 \frac{\kappa_e}{T}(T_c)$, and $\frac{\kappa_e}{T}(T_c) \simeq \frac{\kappa_e}{T}(T \rightarrow 0)$.

Each of these quantitative results, which are independent one from the other, can be a coincidence. The immediate question is whether it is possible to have four independent coincidences?

This question, however, cannot argue strongly in favor of the electronic scenario. In order to decide for one scenario or the other, one should carry out more experiments.

Bibliography

- [1] N.W. Ashcroft and N.D. Mermin, in *Solid State Physics* ch. 8 (Saunders College, 1976).
- [2] R. Berman, in *Thermal Conduction in solids*. ch. 10 (Clarendon Press. Oxford, 1976).
- [3] T. Matsumara and M. J. Laubitz, *Can. j. of Phys.* **48**, 1499 (1970); G.K. White and S.B. Wood, *Phil. Trans. Roy. Soc.* **251**, 273 (1959).
- [4] H.M. Rosenberg, in *Low Temperature Solid State Physics* (Clarendon Press. Oxford, 1963).
- [5] P.D. Thacher, *Phys. Rev.* **156**, 975 (1967)
- [6] H.K. Onnes and G. Holst, *Leiden Comm.* 142c: 126 (1914)
- [7] W.J. de Haas and H. Bremmer, *Proc. Kon. Akad. Wet. Amst.* **34** 325: 126 (1931); *physica* **3** 672, 687:126 (1936)
- [8] K. Mendelson and R.B. Pontius, *Phil. Mag.* **24** 777: 126 (1937)
- [9] C.J. Gorter and H.B.G. Casimir, *Phys. Z.* **35**, 963 (1934).
- [10] J. Bardeen, G. Rickayzen and L. Tewordt, *Phys. Rev.* **142**, 146 (1966).
- [11] L. Tewordt, *Phys. Rev.* **129**, 657 (1963).
- [12] H.M. Rosenberg, *Phil. Trans.* **247**, 441: 119, 129 (1955).
- [13] J.K. Hulm, *Proc. Roy. Soc. A* **204**, 98: 116, 129 (1950).
- [14] L.G. Radosevich and W.S. Williams, *Phys. Rev.* **188**, 770 (1969)
- [15] G. Burns, in *High Temperature Superconductivity, An introduction.* (Academic Press inc. 1992)
- [16] J.G. Daunt and K. Mendelson, *Nature* **141** 116: 128, 277 (1938); *Proc. Roy. Soc. A* **185** 225: 128, 277 (1946)

- [17] for a review see C. Uher in *Physical Properties of High Temperature Superconductors III*. Edited by D. Ginsberg (World Scientific, Teaneck, NJ 1992).
- [18] R.C. Yu, M.B. Salamon, Jian Ping Lu and W.C. Lee, *Phys. Rev. Lett.* **69**, 1431 (1992)
- [19] J.L. Cohn, E.F. Skelton, S.A. Wolf, J.Z. Liu and R.N. Shelton, *Phys. Rev. B* **45**, 13144 (1992)
- [20] J.P. Rice *et al.*, *Phys. Rev. B* **44**, 10158 (1991); D.M. Ginzberg *et al.*, in *The Physics and Chemistry of Oxide Superconductors*, Tokyo, Japan, 16-18 January 1991, edited by Y. Iye and H. Yasuka (Springer, Berlin, 1992).
- [21] T.A. Friedmann, M.W. Rabin, J. Giupitzakis, J.P. Rice and D.M. Ginzberg, *Phys. Rev. B* **42**, 6217 (1990)
- [22] S.E. Stupp and D.M. Ginzberg, in *Physical Properties of High Temperature Superconductors III*. Edited by D. Ginsberg (World Scientific, Teaneck, NJ 1992).
- [23] D.B. Tanner and T. Timusk, in *Physical Properties of High Temperature Superconductors III*. Edited by D. Ginsberg (World Scientific, Teaneck, NJ 1992); D.B. Romero *et al.*, *Phys. Rev. Lett.* **68**, 3305 (1991); M. C. Nuss *et al.*, *Phys. Rev. Lett.* **66**, 3305 (1991)
- [24] W.S. Williams, *Solid State Commun.* **87**, 335 (1993)
- [25] D.A. Bonn, P. Dosanjh, R. Liang and W.N. Hardy, *Phys. Rev. Lett.* **68**, 2390 (1992)
- [26] J.L. Cohn, V.Z. Krezin, M.E. Reeves and S.A. Wolf, *Phys. Rev. Lett.* **71**, 1657 (1993).
- [27] R. Gagnon, C. Lupien and L. Taillefer, *Phys. Rev. B* (Aug. 1994)
- [28] S.J. Hagen *et al.*, *Phys. Rev. B* **40**, 9389 (1989); M. Sera *et al.*, *Solid State Commun.* **74**, 951 (1990); M.F. Crommie and A. Zettle, *Phys. Rev. B* **43**, 408 (1991); D.T. Morelli *et al.*, *Phys. Rev. B* **41**, 2520 (1990)
- [29] U. Welp, S. Flesher, W.K. Wok, J. Downey, Y. Fang, G.W. Crabtree and J.Z. Liu, *Phys. Rev. B* **42**, 10189 (1990)
- [30] J.P. Rice, B.G. Pazol, D.M. Ginzberg, T.J. Moran and M.B. Weissman, *J. Low Temp. Phys.* **72**, 345 (1988)
- [31] Th. Wolf, W. Goldacker, B. Obst, G. Roth and R. Flukinger, *J. Cryst. Growth* **96**, 1010 (1989)
- [32] R. Liang, P. Dosanjh, D.A. Bonn, D.J. Barr, J.F. Carolan and W.N. Hardy, *Physica C* **195**, 51 (1992)

- [33] R. Gagnon, M. Oussena and M. Aubin, *J. Crystal Growth* **114**, 186 (1991)
- [34] T.A. Vanderah, C.K. Lowe-Ma, D.E. Bliss, M.W. Decker, M.S. Osofsky, E.F. Skelton and M.M. Miller, *J. crystal Growth* **118**, 385 (1992)
- [35] J.R. Lagraff and D.A. Payne, *Physica C* **212**, 478 (1993)
- [36] P. Schleger, W.N. Hardy and B.K. Yang, *Physica C* **176**, 261 (1991)
- [37] R. Gagnon, M. Oussena and M. Aubin, *J. Crystal Growth*, **121**, 559 (1992)
- [38] G.K. White, in *Experimental Techniques in Low Temperature Physics*. (Clarendon Press. Oxford 1968)
- [39] D.A. Bonn, private communication.
- [40] C.D. Bredl, K. Peterson, S. Arnold, G. Sparn, F. Steglisch, S. Takahashi, M. Tachiki, B. Runtsch and T. Wolf, *Z. Phys. B* **86**, 187 (1992)
- [41] K. Zhang, D.A. Bonn, S. Kamal, R. Liang, D.J. Baar, W.N. Hardy, D. Basov and T. Timusk, to be published.